10-2002

The Aminopeptidase From *Aeromonas proteolytica*: Structure and Mechanism of Co-Catalytic Metal Centers Involved in Peptide Hydrolysis

Richard C. Holz
Marquette University, richard.holz@marquette.edu

Coordination Chemistry Reviews, Vol. 232, No. 1-2 (October 2002): 5-26. DOI.

The Aminopeptidase from *Aeromonas proteolytica*: Structure and Mechanism of Co-catalytic Metal Centers Involved in Peptide Hydrolysis

Richard C. Holz

Department of Chemistry and Biochemistry, Utah State University, Logan, UT

Abstract

Enzymes containing multi-metal active sites are central to numerous biological processes and, consequently, characterization of their structure and function is a problem of outstanding importance. One of the least-explored groups of enzymes is the hydrolases that contain dinuclear metal centers. These enzymes play key roles in carcinogenesis, tissue repair, and protein degradation processes. In addition, some of these enzymes can catalyze the hydrolysis of phosphorus(V) compounds found in nerve gases and agricultural neurotoxins. The determination of detailed reaction mechanisms for these enzymes is required for the design of highly potent, specific inhibitors that can function as potential pharmaceuticals. Hydrolytic enzymes that contain dinuclear

centers can use every first row divalent transition metal ion from manganese to zinc, except copper. In order to understand the role of each metal ion in catalysis and the apparent non-selectivity of these enzymes towards divalent transition metal ions, it is critical that the reaction mechanism of a prototypical system be determined. The aminopeptidase from *Aeromonas proteolytica* (AAP) is one of the best mechanistically characterized hydrolytic enzymes that contains a dinuclear center and is, therefore, the focus of this review.

Keywords

Aminopeptidase, *Aeromonas proteolytica,* Hydrolases

1. Introduction

Hydrolases that contain dinuclear metal centers catalyze diverse reactions such as the degradation of DNA, RNA, phospholipids, and polypeptides [1], [2], [3], [4], [5]. They are therefore, key players in carcinogenesis, tissue repair, protein maturation, hormone level regulation, cell-cycle control, and protein degradation processes. In addition, metallohydrolases that contain dinuclear active sites are involved in the degradation of agricultural neurotoxins, urea, β-lactam containing antibiotics, and several phosphorus(V) materials used in chemical weaponry [6], [7], [8]. Many metallohydrolases with co-catalytic active sites retain some catalytic activity as mononuclear enzymes but typically exhibit faster rates with dinuclear active sites. The fact that some hydrolases utilize a mononuclear center while others can function with either a mononuclear or dinuclear active site, and still others require two metal ions to catalyze the same chemical reaction, is not well understood. The importance of understanding the mechanism of action of hydrolytic enzymes that contain dinuclear active sites is underscored by the observations that a eukaryotic metallo-aminopeptidase is the target for the antitumor drugs ovalicin and fumagillin [9], [10], [11], [12], [13]. In addition, the naturally occurring peptide analog inhibitor, bestatin, was recently shown to significantly decrease HIV infection in males by inhibiting aminopeptidase activity [14]. For these reasons, several metallohydrolases that contain co-catalytic active sites have become the subject of intense efforts in inhibitor design.

Hydrolases that contain dinuclear active sites utilize a wide range of first row transition metal ions whose structural properties (e.g. coordination geometry and ligand type) regulate their Lewis acidities, which in turn, controls the level of hydrolytic activity (Table 1). Possible roles for one or both metal ions in hydrolases that contain co-catalytic active sites include: (i) to bind and position substrate; (ii) to bind and activate a water molecule to yield an active site hydroxide nucleophile; and/or (iii) to stabilize the transition-state of the hydrolytic reaction. Despite their ubiquity and the considerable structural information available, little was known about how these structural motifs relate to function, until recently. A comparison of the one and two metal-containing peptidases with known X-ray crystal structures, reveals some common features for both mono- and dinuclear hydrolases [1], [15], [16], [17]. All have at least one bound water molecule and many have a non-metal coordinating carboxylate residue, usually a glutamate, that forms a hydrogen bond to a metal-bond water molecule. In order to understand the role of each metal ion in catalysis, it is important that a detailed reaction mechanism of a prototypical hydrolytic enzyme with a dinuclear active site to be elucidated. With this in mind, the focus of this review is the aminopeptidase from *Aeromonas proteolytica* (AAP), primarily because its mechanism of action is one of the best characterized of any hydrolytic enzyme with a co-catalytic metallo-active site. With a detailed reaction mechanism in hand, several potent inhibitors have been designed and synthesized and their binding modes to AAP have been determined. Understanding the reaction mechanism of a prototypical hydrolytic enzyme that contains a dinuclear active site also provides a starting point for the determination of reaction mechanisms for other, less well-understood hydrolases with dinuclear active sites as well as model complex systems. These data in turn, allows new molecules to be designed and synthesized that can be screened as potential pharmaceuticals that target hydrolytic enzymes that bind two metal ions in a co-catalytic site.

Table 1. Selected X-ray crystallographically characterized hydrolytic enzymes with dinuclear active sites

Enzyme	Function	Metal	References
Bovine lens leucine aminopeptidase	N-Terminal amino acid hydrolysis	Zn(II)	[18]
Aminopeptidase from *Aeromonas proteolytica*		Zn(II)	[19]
Aminopeptidase from *Streptomyces griseus*		Zn(II)	[20]
Aminopeptidase P		Mn(II)	[21]
Methionyl aminopeptidases		Fe(II) of Co(II),	[22]
Carboxypeptidase G_2	Folates to pteroates and l-glutamate	Zn(II)	[23]
Alkaline phosphatase	Phosphate monoester hydrolysis	Zn(II)/Mg(II)	[24]
Phospholipase C	Phosphatidylcholine hydrolysis	Zn(II)/Mg(II)	[25]
P1 Nuclease	Phosphate diester hydrolysis	Zn(II)/Mg(II)	[26]
Purple acid phosphatases	Phosphate ester hydrolysis	Fe(III/II)	[27]
Phosphotriesterase	Organophosphate ester hydrolysis	Zn(II)	[28]
Arginase	Hydrolysis of l-arginine	Mn(II)	[29]
Enolase	Hydrolysis of 2-phospho-d-glycerate	Mn(II)	[30]
β-Lactamase	β-Lactam degradation	Zn(II)	[31]
Urease	Hydrolysis of urea	Ni(II)	[32]

2. Leucine aminopeptidase from *Aeromonas proteolytica*

Aminopeptidases are a group of exopeptidases that catalyze the hydrolysis of a wide range of N-terminal amino acid residues from proteins and polypeptides [33], [34], [35]. The aminopeptidase from *Aeromonas proteolytica* (EC 3.4.11.10) (AAP) possesses ideal properties for studying hydrolytic reactions catalyzed by hydrolases that bind two metal ions in a co-catalytic site [36]. AAP is a small, monomeric enzyme (29.5 kDa) that contains two Zn(II) ions per mole of polypeptide [36]. These data are in contrast to a number of bacterial and mammalian aminopeptidases that are hexameric with total molecular weights ≥600 kDa [37], [38]. AAP was first purified from culture filtrates of the marine bacterium *A. proteolytica* (ATCC 15338) in 1966 [39]. AAP was shown to be an unusually stable enzyme; it retains its activity at 70 °C for several hours, and is only partially inactivated in 8 M urea [36], [40]. These properties facilitated the purification of AAP, since other proteases co-purified with AAP can be inactivated via extensive heat treatment. Prescott et al. [41] showed that the complete removal of the two zinc ions from AAP quenched the enzymatic activity but the re-addition of one mole of Zn(II) restored ∼80% of the original enzymatic activity. The first bound Zn(II) ion was also shown to posses a dissociation constant of $\sim 1.5\times10^{-10}$ M. AAP was only very recently overexpressed in *Escherichia coli* as a 42 kDa enzyme that is then proteolytically processed to the fully active 29.5 kDa form [42].

The hydrolysis of l-leucine-*p*-nitroanilide (l-*p*NA) by AAP, the most widely used leucine aminopeptidase substrate, was studied as a function of pH [43]. k_{cat} was found to increase between pH 4 and 5.5 above which k_{cat} was invariant up to pH 11; however, the value of K_m was pH dependent between 6 and 10. At pH 6, K_m was found to be 45 μM but decreased to 19 μM at pH 8. The value of K_m remained constant between pH 8.0 and 9.5 but increased slightly to 25 μM at pH 10 [43]. Based on k_{cat}/K_m values determined over the pH range 4–11, the pK_a value for a putative Zn(II)-bound hydroxide was suggested to be 4.8. However, it was later suggested that at a pH value of 4.8 the change in K_m actually reflected Zn(II) ion binding to AAP [40]. Baker and Prescott [43] noted that excess Zn(II) was required at pH values less than 6.5 because of observed decreases in

activity levels due to the loss of metal ions. Since the active site of AAP is carboxylate rich, the pK_a value of 4.8 likely reflects the deprotonation of glutamate or aspartate residues that function as ligands since it is well known that these amino acid residues have pK_as between 4.5 and 5.0 [19].

The X-ray crystal structure of AAP was solved in 1992 by Chevier et al. [19] to 1.8 Å resolution. The structure revealed an eight-stranded β-sheet surrounded by eight, structurally equivalent α-helices (Fig. 1). Since AAP is an enzyme with a mass of only 29.5 kDa, the β-sheet and α-helical content make up over 50% of the amino acids in the polypeptide chain. Prescott and Wilkes [36] previously reported that AAP retained ~50% of its enzymatic activity in 8 M urea suggesting that AAP is not fully denatured under these conditions. The dinuclear active site of AAP resides close to the surface of the enzyme, adjacent to a hydrophobic pocket. A single disulfide bond exists at the back of the hydrophobic pocket essentially holding the two halves of the enzyme together [19]. The co-catalytic active site contains a (μ-aquo)(μ-carboxylato)dizinc(II) core with a terminal carboxylate and histidine residue ligating each metal ion resulting in symmetric coordination spheres for the dinuclear cluster (Fig. 2). Both zinc ions reside in a distorted tetrahedral coordination geometry with a Zn□Zn distance of 3.5 Å. An oxygen atom of Glu151 forms a hydrogen bond with the bridging water molecule while the second oxygen atom is 3.4 Å from the N^{ε} of His97 which is a ligand to Zn1 (Fig. 3).

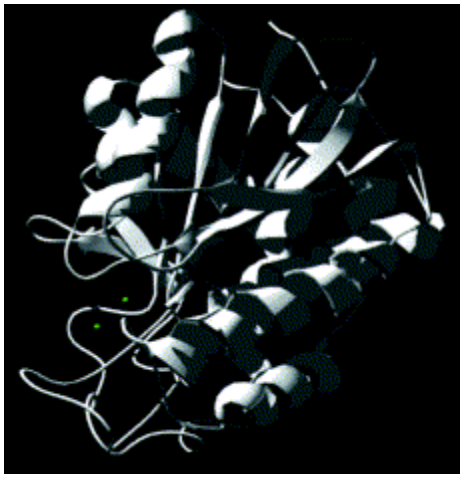

Fig. 1. Ribbon diagram of the X-ray crystal structure of AAP based on the coordinates from the Protein Data Bank (1AMP). The two zinc(II) ions are depicted as green spheres.

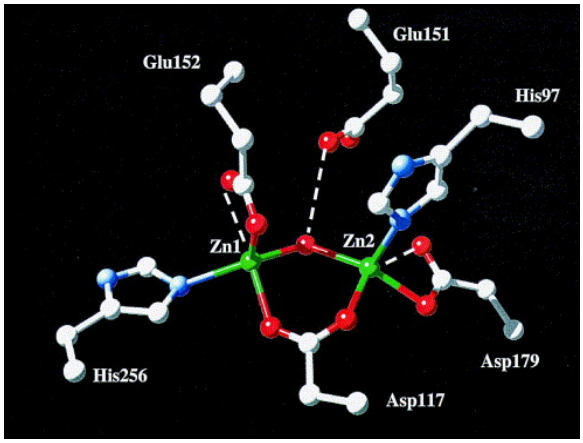

Fig. 2. Schematic of the native AAP active site based on the coordinates 1AMP. Glu151, also shown, is not a metal ligand but is thought to participate in the hydrolytic reaction.

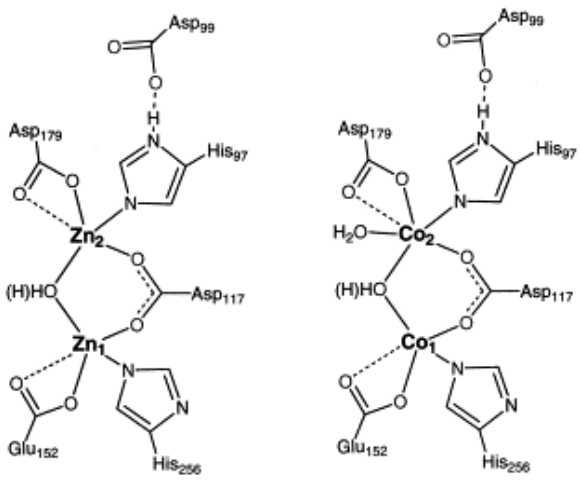

[ZnZn(AAP)] **[CoCo(AAP)]**

Fig. 3. Drawing of the active site of [ZnZn(AAP)] along with the proposed active site geometry of [CoCo(AAP)] based on spectroscopic studies.

Substitution of the two g-atoms of Zn(II) in AAP with Co(II), Cu(II), or Ni(II) provides varying levels of activity that are dependent on the order of addition [44], [45]. The Cu(II), Co(II), and Ni(II)-substituted enzymes are hyperactive by 6.5, 7.7, and 25 times, respectively. The addition of one mole of Cu(II), Co(II), or Ni(II) to the apo-enzyme followed by the addition of Zn(II) enhances the enzymatic activity to an even greater extent. For Ni(II) and Cu(II), nearly a 90- and 100-fold increase in activity was observed, respectively, relative to the dizinc(II) center. Alterations in the catalytic efficiency of AAP were not limited to k_{cat} alone, since the enzyme's affinity for substrate changed as a function of the mixed-metal combination. For the heterodimetallic enzymes, metal exchange was reported not to occur during the time course of kinetic experiments and samples could be frozen and thawed without loss in specific activity [45].

2.1. Spectroscopic characterization of Co(II)-loaded AAP

Zn(II) has a full complement of d-electrons (10) making it both magnetically and spectroscopically silent. The ligand-field stabilization energies (LFSEs) for both octahedral (O_h) and tetrahedral (T_d) geometries of Zn(II) are zero, suggesting that neither structure is favored. However, based on X-ray crystallographic data, Zn(II) clearly favors a T_d geometry [46]. The reason for this is that the 4s and 4p orbitals are easily accessible as electron-pair acceptors, providing an sp^3-type center, while the 5d orbitals are higher in energy making the formation of O_h or trigonal bipyramidal (TBP) complexes slightly less favorable. LFSEs suggest that Co(II) also favors T_d complexes by $(2/5)\Delta_o$ [47]. Since Co(II) has an ionic radius similar to that of Zn(II) (0.74 vs. 0.75 Å), has seven d-electrons, and is paramagnetic (S=3/2) Co(II) has been shown to be an excellent probe of Zn(II) containing metalloproteases [48]. In fact, several Zn(II)-metalloproteases with similar active site ligands to those of AAPs have been substituted with Co(II) in vitro and, in nearly all cases, active and even hyperactive enzymes are obtained [48], [49]. Therefore, the substitution of Zn(II) with the spectroscopically active transition metal ion Co(II), is an important and necessary step for the spectroscopic characterization of mechanistic steps.

The addition of one equivalent of Co(II) to AAP provides an enzyme that exhibits ~80% of the specific activity of the dicobalt(II) form [44], [45]. Similar observations have also been made for the Zn(II)-loaded enzyme. Based on these data, the roles of Co(II) and Zn(II) appear to be similar in AAP. Electronic absorption spectra of AAP in the presence of one and two equivalents of Co(II) (referred to as [Co_(AAP)] and [CoCo(AAP)]) (Fig. 4) were first recorded by Prescott et al. [50], [51]. The addition of one Co(II) ion to AAP at pH 7.5, provides a visible

absorption spectrum with a band at 525 nm (ε_{525}~50 M^{-1} cm^{-1}). Addition of a second equivalent of Co(II) increases the absorption intensity at 525 nm to ~90 M^{-1} cm^{-1}. The addition of more than two equivalents of Co(II) does not alter the intensity or position of the observed absorption band. The added absorptivity ($\Delta\varepsilon_{525}$ of ~40 M^{-1} cm^{-1}) appears to be due to a broad underlying protein absorption band that is not due to Co(II) absorption. A similar broad absorption band was observed for the Co(II)-substituted R2 subunit of ribonucleotide reductase, and is also evident in several Co(II) model complexes [52]. Therefore, the increase in absorption at 525 nm due to the second Co(II) ion is only ~20 M^{-1} cm^{-1}.

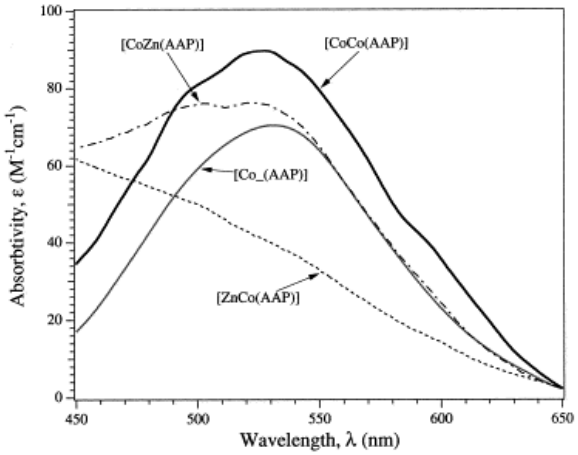

Fig. 4. Electronic absorption spectra of [CoCo(AAP)], [Co_(AAP)], [CoZn(AAP)], and [ZnCo(AAP)] in 50 mM HEPES buffer at pH 7.5 containing 150 mM KCl.

Ligand-field theory predicts that d–d transitions of four coordinate Co(II) complexes give rise to intense absorption (ε>300 M^{-1} cm^{-1}) in the higher wavelength region of 625±50 nm owing to a comparatively smaller LFSE, while transitions of octahedral Co(II) complexes have very weak absorption (ε<30 M^{-1} cm^{-1}) at lower wavelengths (525±50 nm) [48]. A five-coordinate Co(II) ion shows intermediate features: i.e. moderate absorption intensities (50<ε<250 M^{-1} cm^{-1}) with several maxima between 525 and 625 nm [48], [53]. The molar absorptivities and absorption maxima of [Co_(AAP)] and [CoCo(AAP)] are consistent with the first Co(II) ion residing in a distorted tetrahedral or a distorted trigonal bypyramidal coordination environment while the second Co(II) ion is likely octahedral (Fig. 3) [50]. These conclusions were also supported by magnetic circular dichroism (CD) spectra [50].

The active sites of several metalloenzymes have been probed by electron paramagnetic resonance (EPR) spectroscopy of their S=3/2 high-spin Co(II)-substituted derivatives. Recently, a new systematic protocol for the interpretation of Co(II) EPR spectra was developed and the S=3/2 spin states of the Co(II)-substituted forms of AAP were characterized [51], [54]. This protocol allows the simulation of line-shape using theoretically allowed g_{eff} values, corresponding to an isotropic g_{real} value, by treating high-spin Co(II) ions as an effective S=1/2 system. Since Co(II) ions in either tetrahedral or octahedral ligand-fields typically exhibit extensive spin–orbit coupling, large zero-field splitting (E/D) is observed (Fig. 5) [55]. In addition, the gross distortion of EPR spectra of high-spin S=3/2 Co(II) ions was investigated along with the effects of saturation on line-shape and on simulation-derived spectral parameters. For [Co_(AAP)], a distinctive EPR signal was observed in which the ^{59}Co hyperfine pattern was not centered on the low-field absorption (Fig. 5) [51]. This signal could not be simulated as a single species but subtraction of EPR spectra recorded at different temperatures revealed that two species were present. The first species exhibited an axial signal with g_{eff} values of 5.75, 4.50, and 2.50. These values correspond to an M_s=1±1/2> ground state transition with g_{real}=2.57 and E/D=0.08. The second species had g_{eff} values of 6.83, 2.95, and 1.96 and exhibited a characteristic eight-line ^{59}Co hyperfine pattern

with A_z=7.2 mT, g_{real}=2.57, and E/D=0.28. The possibility that these spectra were due to contributions from M_s=1±1/2> and 1±3/2> doublets of a single spin system was investigated, but subtraction of spectra recorded at various temperatures clearly indicated that the features at g=2.95 and 1.96 were correlated with the feature at g=6.83. Furthermore, at temperatures above 15 K, the signal intensity rapidly decreased and both signals were lost.

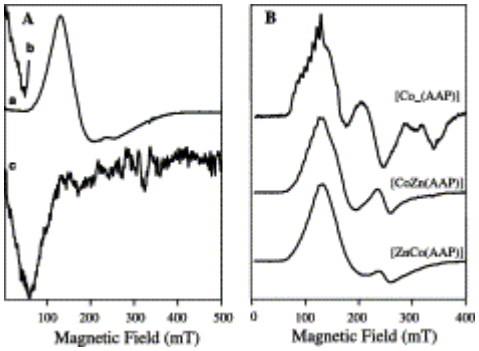

Fig. 5. (A) S=3/2 and 3 EPR signals from [CoCo(AAP)]. Spectrum a is the perpendicular mode EPR signal from a sample of AAP containing 1.5 equivalents of Co(II). Spectrum a was recorded at 10 K, 0.2 mW microwave power. Inset b: the low-field region of spectrum a plotted with a 32-fold increase in signal intensity. Spectrum c is the parallel-mode EPR signal of the same sample recorded at 4.2 K, 5 mW microwave power. (B) EPR spectra of [Co_(AAP)], [CoZn(AAP)], and [ZnCo(AAP)] recorded at 10 K, 0.2 mW microwave power.

The EPR spectrum of [CoCo(AAP)] was also recorded and simulated as a single axial species with g_{eff} values of 5.10, 3.84, and 2.18; M_s=1±1/2>, g_{real}=2.25, E/D=0.1 (Fig. 5) [51]. The intensity of this signal corresponded to 0.13 spins per mole of Co(II) indicating that the two Co(II) ions in AAP experience significant spin–spin interaction. Perpendicular mode EPR titration of apo-AAP with Co(II) revealed a low-field signal extending out of zero-field in samples with more than one equivalent of Co(II) added. Coincident with the appearance of this low-field perpendicular mode signal was the appearance of a parallel-mode EPR signal with g∼12. These data indicate that the two high-spin S=3/2 Co(II) ions in the dinuclear active site of AAP are ferromagnetically coupled. The existence of an S=3/2 perpendicular mode signal in [CoCo(AAP)] samples that also exhibit an S=3 parallel-mode signal provided evidence for a population distribution of S=3/2 and 3 species. The presence of mixed magnetic species in Co(II)-substituted proteins is not uncommon and in some cases can be related to the sensitivity of the EPR parameters to angular co-orientational microheterogeneities.

Inspection of the observed EPR spectra for [Co_(AAP)] and [CoCo(AAP)] indicates that two species are present in solution for [Co_(AAP)] and that these two species can be differentiated and simulated. Based solely on the EPR data the coordination number and geometry of the Co(II) ions in [Co_(AAP)] and [CoCo(AAP)] cannot be determined. As Johnson and coworkers pointed out, the presence or absence of resolvable ^{59}Co hyperfine structure is not an indication of coordination geometry since both tetrahedral and octahedral complexes exhibit ^{59}Co hyperfine structure [56]. Moreover, Pilbrow and Hanson [57] showed theoretically that the magnitude of ^{59}Co hyperfine structure is effectively independent of the Co(II) ion coordination geometry. Empirical relationships between EPR parameters and coordination geometry for high-spin S=3/2 Co(II) ions are also difficult to deduce, primarily because of a lack of reliable EPR parameters for Co(II) coordination complexes in the literature. Therefore, the only direct geometrical information available from EPR is the extent of deviation from idealized axial geometry as indicated by the rhombic distortion, E/D, of the axial zero-field splitting.

Comparison of the EPR data of [Co_(AAP)] and [CoCo(AAP)] with the previously reported electronic absorption data, suggest that the difference between the two EPR active species in [Co_(AAP)] is not likely one of coordination number. This must also be the case for [CoCo(AAP)] since the second Co(II) ion clearly resides in an

octahedral environment with a small (~10 M^{-1} cm^{-1}) molar absorptivity. The two species observed in the EPR spectra of [Co_(AAP)] appear to be the result of constraints imposed on the Co(II) ion coordination geometry by the ligand-field. For example, the signal exhibiting resolvable ^{59}Co hyperfine splitting is likely due to a Co(II) ion in a highly constrained and asymmetric coordination geometry. That the geometry is asymmetric is clearly evident from the anisotropy of the EPR spectrum (E/D=0.28). Furthermore, the high g_{real} value of 2.57 is indicative of a high degree of spin–orbit coupling, as would be expected for a high-spin Co(II) ion in a coordination environment with low symmetry. A highly constrained geometry is also evident from the resolvable ^{59}Co hyperfine splitting in that the EPR linewidth has to be narrow enough and not significantly broadened by factors such as *g*-strain which arise from micro-distributions in the Co(II) coordination environment. In the case of the ^{59}Co hyperfine-split signal, it is evident that the variability in the structure of the species responsible must be small, again indicating a highly constrained Co(II) environment.

In contrast, the second species appears to be due to a Co(II) center with much less constraint upon its geometry. The less rhombically distorted EPR spectrum (E/D=0.08) indicates a significantly more symmetrical environment. Such an environment is likely the result of relaxation of ligand sphere-derived constraints. Consistent with the adoption of such a coordination geometry being due to the relaxation of the ligand-field, a wider distribution of microheterogeneous structures in a given sample is observed. The deviation of g_{real}=2.57 from the free electron value of 2.0 is required by spin–orbit coupling, which will be uniformly small in axially symmetric systems. In most cases, axial symmetry will be adopted by systems with a high degree of flexibility that allows the coordination geometry to adopt the lowest energy. However, a number of other slightly higher energy conformations exist into which the complex can be excited by thermally induced vibrational modes. It is reasonable to expect that for an axially symmetric Co(II) species, the distribution of microheterogeneous environments will be relatively wide and the resultant *g*-strain in the EPR spectrum will preclude the observation of ^{59}Co hyperfine splitting, although the hyperfine interaction is still present. It is worth noting that although the broad axial species of [Co_(AAP)] and [CoCo(AAP)] superficially may appear to resemble signals observed in other Co(II) systems including $[Co(H_2O)_6]^{2+}$, computer simulation has shown that each of these signals has distinct EPR parameters. Similarity in the appearance of these signals should not be over interpreted since the EPR spectra of any essentially axial Co(II) ion will closely resemble each other because the g_{eff} values are dictated by g_{real} and E/D. Therefore, correlation of either coordination number or geometry in species exhibiting similar EPR spectra should not be assumed, whereas the symmetry of the electronic field can be inferred.

Investigation of the appearance of the g~12 parallel-mode EPR by titrating apo-AAP with Co(II), allowed Bennett and Holz to demonstrate that metal binding to apo-AAP occurred in a sequential fashion [51]. For AAP samples that contained less than one equivalent of Co(II) no g~12 signal was observed. As more Co(II) was added, the intensity of this feature was found to increase linearly between one and two equivalents with no further increase in intensity being observed beyond two equivalents of added Co(II). Since exchange-coupling was only observed after one equivalent of added Co(II), metal binding to AAP occurs sequentially. These data highlight the potential formation of heterodimetallic sites. Catalytically competent heterodimetallic centers provide systems in which the function of each metal ion can be independently studied by labeling the metal binding sites with spectroscopically active and silent metal ions, respectively. For example, [CoZn(AAP)] and [ZnCo(AAP)] can be prepared and each provides a spectroscopically distinct signature (Fig. 5) [50], [54].

Electronic absorption spectra were recorded for [CoZn(AAP)] and [ZnCo(AAP)] and the component due to apo-AAP was subtracted [50], [54]. For [CoZn(AAP)], a visible absorption spectrum with a broad band at 525 nm (ε_{525}~50 M^{-1} cm^{-1}) was obtained which is identical to that of [Co_(AAP)]. The addition of one equivalent of Zn(II) followed by one equivalent of Co(II) to apo-AAP provided an absorption spectrum with very little clear absorption around 525 nm due to Co(II) (~10 M^{-1} cm^{-1}). The molar absorptivities and absorption maxima of the electronic absorption spectra of [CoZn(AAP)] and [ZnCo(AAP)] are consistent with the first Co(II) ion residing in a

tetrahedral or possibly five-coordinate environment while the second Co(II) ion is octahedral. The EPR spectrum of [CoZn(AAP)] was also recorded and provided a spectrum consistent with a high-spin *S*=3/2 Co(II) center; however, the eight-line hyperfine pattern due to the *I*=7/2 ^{59}Co nucleus was not centered on the low-field absorption feature [54]. This feature, along with the presence of a derivative shaped feature at 243 mT, clearly indicated the presence of more than one signal and, not surprisingly, this signal could not be simulated as a single species. The EPR spectrum of [ZnCo(AAP)] provided an EPR signal distinct from that observed for [CoZn(AAP)]. Again, a weak hyperfine pattern due to ^{59}Co was observed for [ZnCo(AAP)] but was not centered on the low-field absorption feature indicating that more than one species was present. The differences between the EPR spectra of [CoZn(AAP)] and [ZnCo(AAP)] at pH 7.5 were subtle but corroborate the more dramatic evidence from electronic absorption spectroscopy indicating that the two metal binding sites can be selectively labeled.

Subtraction of EPR spectra of [CoZn(AAP)] recorded at pH 7.5 and pH 10 revealed that two species were present and that the relative contributions were dependent on the pH. On the other hand, the EPR spectrum of [ZnCo(AAP)], which also contained two species, exhibited little pH dependence and individual species could not be isolated [54]. Comparison of the EPR signals observed for [CoZn(AAP)] and [ZnCo(AAP)] at pH 10 with those observed for [Co_(AAP)] and [CoCo(AAP)] at pH 10 revealed some striking similarities and differences [54]. Similar to [CoZn(AAP)], EPR spectra of [Co_(AAP)] recorded at pH 10 exhibited a marked increase in the ^{59}Co hyperfine signal and a decrease in the intensity of the broad axial signal. On the other hand, EPR spectra of [CoCo(AAP)] recorded at pH 10 were indistinguishable from those recorded at pH 7.5. However, as the pH was increased from 5.9 to 10.0, the intensity of the *S*=3 parallel-mode EPR signal, due to ferromagnetic coupling between the two Co(II) ions, decreased. Concomitant with the loss of the *S*=3 signal, an increase in the *S*=3/2 signal intensity due to [CoCo(AAP)] was observed. Therefore, an ionizable group mediates spin-coupling between the two Co(II) centers and perturbs the metal ion bound to the first metal binding site, but had little effect on the second metal binding site. Inspection of the X-ray crystal structure of [ZnZn(AAP)] reveals a single oxygen atom bridge between the two Zn(II) ions at pH 7.0 [19]. One possible explanation for the presence of two species in Co(II)-substituted AAP would be the existence of a bridging water molecule that is in equilibrium with a terminal hydroxide (Scheme 1). Thus, as the pH is increased, a higher proportion of the Co(II) ions in a population of [CoZn(AAP)] interacts with an hydroxyl group and this interaction constrains the geometry of the Co(II) ion. This proposal is consistent with the EPR data in that a greater percentage of the ^{59}Co hyperfine-split signal is observed at high pH values for both [Co_(AAP)] and [CoZn(AAP)] which is due to a Co(II) ion in a highly constrained and asymmetric coordination geometry [54]. That the geometry is asymmetric for these two species is clearly evident from the anisotropy of the EPR spectrum (*E*/*D*=0.28 and 0.32, respectively).

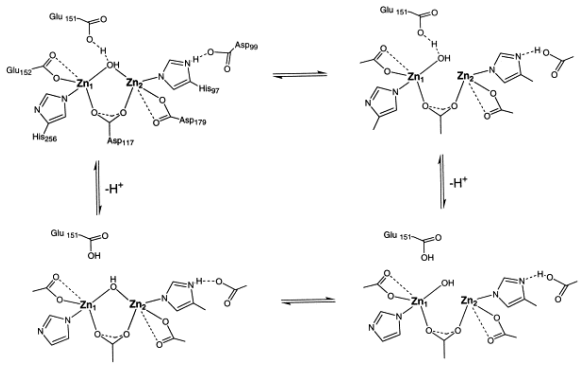

Scheme 1.

2.2. The first step in catalysis, substrate binding

AAP has been shown to require peptide substrates with a free α-amino-group in the l-configuration and prefers hydrophobic residues in the NH_2-terminal position [36], [38], [58], [59], [60], [61], [62]. AAP will hydrolyze di- and tripeptides as well as amino acid amides, esters, β-napthylamides, and *p*-nitroanilides [36]. Based on X-ray crystallographic studies, a well defined hydrophobic pocket is adjacent to the dinuclear Zn(II) active site of AAP that is made up of Met180, Ile193, Cys223, Tyr225, Cys227, Met242, Phe248, Tyr251, and Ile255 [19]. The two Cys residues form a disulfide bond at the back of this pocket. Based solely on X-ray crystallographic data, this pocket was suggested to accommodate the hydrophobic side chain of the N-terminal residue [19], [63]. Chemical modification studies on AAP suggest that at least one tyrosine residue is important in the catalytic mechanism [64]. At least two tyrosine residues reside in the previously defined hydrophobic pocket. One of these tyrosine residues was initially proposed to deprotonate the Zn(II)-bound water molecule providing the nucleophile in catalysis [64]. However, it was recently proposed that Glu151, which is much closer to the dizinc(II) center based on the X-ray crystal structure and has a pK_a much closer to that of a Zn(II)-coordinated water molecule, is the general acid/base in the catalytic mechanism of AAP. Confirmation of this proposal must await site-directed mutagenesis studies in which these tyrosine residues are mutated to phenylalanine residues. This mutation will delete their ability to form hydrogen bonds, which will likely affect the substrate binding affinity. More likely, the role of these two tyrosine residues in catalysis is substrate recognition by providing hydrogen bonds to assist in positioning the substrate. Chemical modification of these residues probably prevented entry of the substrate into the active site and thus inhibited the catalytic reactivity.

In order to gain insight into the role of the hydrophobic pocket in catalysis, the binding of a series of seven aliphatic and two aromatic alcohols were investigated as reporters of substrate selectivity of AAP (Table 2) [65]. This series of alcohols was chosen to systematically probe the effect of the carbon chain length, steric bulk, and inhibitor shape on the inhibition of AAP. Initially, the question of whether AAP was denatured in the presence of aliphatic alcohols was addressed. Based on CD, electronic absorption, and fluorescence spectra the secondary structure of AAP, with and without added aliphatic alcohols, was shown to be unchanged. These data clearly indicated that AAP is not denatured in aliphatic alcohols, even up to concentrations of 20% (v/v). All of the alcohols studied were competitive inhibitors of AAP with K_i values between 860 and 0.98 mM. The clear trend in the data was that as the carbon chain length increased from one to four, the K_i values revealed tighter binding. Branching of the carbon chains also caused tighter inhibitor binding but large bulky groups, such as that found in *tert*-butanol, do not inhibit AAP as well as leucine analogs, such as 3-methyl-1-butanol.

Table 2. Summary of the inhibition constants for aliphatic alcohol inhibition of AAP at pH 8.0

Inhibitor	**K_i (mM)**
Methanol	860±20
Ethanol	80±8
n-Propanol	11±2
tert-Butanol	10±2
iso-Propanol	8±2
n-Butanol	2.7±0.3
Phenol	4.0±0.4
Benzyl alcohol	2.6±0.3
3-Methyl-1-butanol	0.98±0.1

The competitive nature of the inhibition of this series of alcohols indicates that the substrate and each alcohol studied are mutually exclusive due to binding at the same site on the enzyme. Based on EPR and electronic absorption data for Co(II)-substituted AAP, none of the alcohols studied perturbed the spectroscopic signatures

indicating that these inhibitors do not bind to the dinuclear active site of AAP. Thus, reaction of the inhibitory alcohols with the catalytic metal ions cannot constitute the mechanism of inhibition. These data suggest that each of these inhibitors binds only to the hydrophobic pocket of AAP (Scheme 2) and, consequently, blocks the binding of substrate. Thus, the first step in peptide hydrolysis is the recognition of the N-terminal amino acid side chain by the hydrophobic pocket adjacent to the dinuclear active site of AAP.

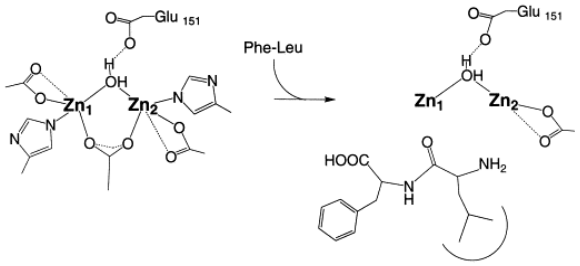

Scheme 2.

2.3. Amine binding versus carbonyl binding

The peptide inhibitor l-leucinethiol (LeuSH) was found to be a potent, slow-binding competitive inhibitor of AAP [66]. The overall potency (K_i*) of LeuSH was 7 nM while the corresponding alcohol l-leucinol (LeuOH) was a simple competitive inhibitor of much lower potency (K_i=17 μM). These data suggest that the free thiol is likely involved in the formation of the E▪I and E▪I* complexes, presumably providing a metal ligand. Electronic absorption spectra of [CoCo(AAP)], [CoZn(AAP)], and [ZnCo(AAP)] in the presence of both inhibitors were recorded [66]. In the presence of LeuSH, all three Co(II)-substituted AAP enzymes exhibited an absorption band centered at 295 nm characteristic of an S→Co(II) ligand–metal charge-transfer band. In addition, all absorption spectra recorded in the range 450–700 showed changes characteristic of LeuSH and LeuOH interacting with both metal ions.

EPR spectra of [CoCo(AAP)]–LeuSH, [ZnCo(AAP)]–LeuSH, and [Co_(AAP)]–LeuSH were recorded at low (3.5–4.0 K) and high temperatures (19 K) over a range of microwave powers [66]. The signals observed at low temperature were unusual and appeared to contain, in addition to the incompletely saturated contributions from the signals characterized at 19 K, a very sharp feature at g_{eff}=∼6.5 that appears to be characteristic of thiolate–Co(II) interactions [67]. A similar $g_{eff.}$=∼6.5, was not observed for any Co(II)-loaded AAP sample bound by LeuOH. The EPR spectrum of [CoCo(AAP)]–LeuSH also indicated that the Co□OH(H)□Co bridge was broken upon reaction with LeuSH since no spin-coupling between the two Co(II) centers was observed. Moreover, these data indicated that LeuSH does not provide an M□μS(R)□M bridge and that the electrophilic N-terminal amine group does not provide a ligand to the non-sulfur-liganded metal ion. Based on these data, it was proposed that the hydrophobic side chain is first recognized by the hydrophobic pocket, followed by carbonyl coordination to the first metal binding site. Due to the lack of amine binding to the second metal ion, carbonyl binding must occur first followed by N-terminal amine binding to the second metal binding site (Scheme 3).

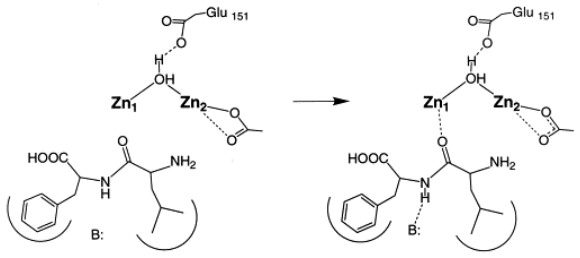

Scheme 3.

2.4. Substrate-analog inhibitors of AAP

Several inhibitors of AAP have been studied and these molecules can be classified into three types: substrate analogs, tetrahedral transition-state analogs, and simple metal-chelating agents. Examples of the former two types include boronic acids [43], [68], [69], chloromethyl ketones [36], and phosphonic acids [18], [70], [71]. Among the metal chelators, hydroxamates [72], [73], [74] and α-hydroxyamides [36] have been shown to be particularly potent inhibitors of AAP. A potential substrate-analog inhibitor, *n*-valeramide, was shown to be a weak competitive inhibitor of AAP with a K_i of 5.2 mM [43]. Electronic absorption studies on *n*-valeramide bound to AAP (23-fold excess of *n*-valeramide) showed no detectable change in the absorption properties of the various Co(II)-loaded homo- and heterodimetallic forms of AAP [50]. Given the fact that the K_i exhibited by *n*-valeramide is similar in magnitude to the aliphatic alcohol 3-methyl-1-butanol [65], which also does not bind to the dinuclear active site it is more likely that *n*-valeramide, like 3-methyl-1-butanol, binds only to the hydrophobic pocket.

1-Butaneboronic acid (BuBA) was reported to be a strong, slow-binding competitive inhibitor of AAP (K_i*=10 μM at pH 8.0) [43]. The binding of several α-aminoboronic acids to aminopeptidases has been shown to be biphasic, slow-binding inhibitors [68], [69]. Electronic absorption spectra of [CoZn(AAP)] and [ZnCo(AAP)] in the presence of BuBA have been recorded [54]. For [CoZn(AAP)]–BuBA, new bands at 480, 500, and 590 nm were observed with a concomitant increase in the molar absorptivity (ε_{527}=55 M^{-1} cm^{-1}) while that of [ZnCo(AAP)] remained unchanged. These data suggest that BuBA coordinates only to the first metal binding site in AAP but does not interact with the second site. The addition of BuBA to [CoZn(AAP)] also resulted in a distinct change in the EPR spectrum; however, addition of BuBA to [ZnCo(AAP)] left the EPR spectrum completely unperturbed [54]. These data are consistent with electronic absorption spectra and indicate that BuBA binds only to the first metal binding site of AAP and does not interact with the second site. Furthermore, the addition of one equivalent of BuBA to [CoCo(AAP)] at pH 7.5, resulted in the immediate loss of the *S*=3 parallel-mode EPR signal suggesting that upon BuBA binding, the μ-aquo bridge between the Co(II) ions is lost [51], [54]. Since AAP is ca. 80% active with only a single Zn(II) ion bound it seems likely that the bridging water molecule becomes terminal upon substrate binding and is bound to a single metal ion (Scheme 4). Thus, the exchange-coupling between the two Co(II) ions is lost and the terminal water/(OH^-) likely represents the nucleophile in the enzymatic reaction.

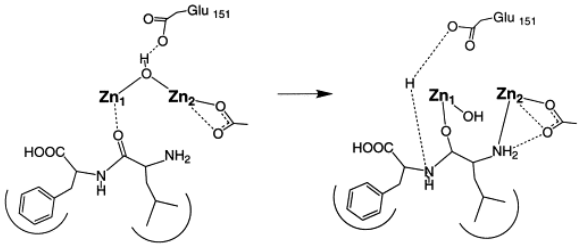

Scheme 4.

The X-ray crystal structure of AAP complexed with BuBA was recently solved at 1.9 Å resolution (Fig. 6) [75]. BuBA binding to AAP does not induce major conformational changes in the protein and the structures of native AAP and the AAP–BuBA complex agree well, with an r.m.s. deviation of 0.17 Å for the 291 structurally equivalent C α-atoms. The two Zn(II) atoms are 3.3 Å apart in the BuBA complex compared to 3.5 Å in the native structure (Fig. 7) [19]. The amino acid residues ligated to the dizinc(II) cluster are identical to those of the native enzyme with only minor perturbations to the bond lengths. The BuBA oxygen atoms are 2.5 and 2.7 Å from Zn1 and 3.0 and 4.4 Å from Zn2 suggesting that BuBA binds only to Zn1 and not to Zn2, consistent with the electronic absorption and EPR data recorded on Co(II)-substituted AAP. Since metal binding to the dinuclear active site has been shown to be sequential and BuBA binds to the Zn1 site, Zn1 can be designated as the first metal binding site to fill upon the addition of metal ions.

Fig. 6. Schematic of BuBA bound to the dinuclear center AAP based on the coordinates from the Protein Data Bank (1CP6). The zinc ions are depicted as green spheres and BuBA as red, magenta, and white spheres.

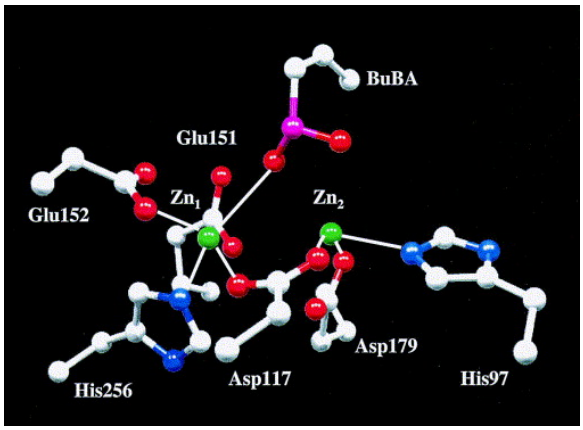

Fig. 7. Schematic of BuBA bound to the dinuclear center AAP based on the coordinates 1CP6. The zinc ions have symmetric coordination spheres in that each has a terminal carboxylate and histidine residue in addition to the bridging aspartate residue. BuBA is bound asymmetrically with respect to the zinc ions.

The X-ray structure also revealed that the boron atom of BuBA is not trigonal planar (sp^2) but is trigonal pyramidal (sp^3). In the absence of enzyme, BuBA was reported to be >99% in the boronic acid form (sp^2 hybridized) at pH 8.0, with a reported pK_a of 10.62 [43]. Therefore, the loss of planarity about the boron atom must be the result of binding to the dinuclear active site of AAP. In addition, there is no electron density near the two Zn(II) ions that would be consistent with a bridging water molecule in the AAP–BuBA complex (Fig. 7) [75]. A new water molecule (water-53) that was not present in the native structure resides 2.4 Å from the boron atom of BuBA. Although rather far from both Zn(II) ions (4.3 Å from Zn1 and 4.8 Å from Zn2), water-53 may in fact represent the nucleophile in the catalytic reaction since it resides on the correct side of the boron atom to have been delivered by Zn1. Moreover, it is well positioned for an in-line attack on the carbonyl carbon atom of the peptide substrate if the N-terminal amino acid residue were bound analogously to BuBA with the carbonyl carbon in the position of the boron atom. Based on these data, it is reasonable to propose that the sp^2 hybridized form of BuBA, binds to the dinuclear active site of AAP via the coordination of O1 to Zn1. This initial Zn(II) binding-step would then be followed by attack of the active site Zn1-bound water/hydroxide to the

electron deficient P_z orbital of the boron atom making it sp^3, similar to nucleophilic attack on a peptide substrate (Scheme 5). These data are consistent with previous kinetic studies on BuBA binding to AAP which indicated that BuBA binds in a two step process [43], analogous to the binding of boronic acids to serine proteases [76], [77]. Therefore, the AAP–BuBA complex represents the proteolytic reaction in an arrested form between the Michaelis complex and the transition-state. This structure of a reaction intermediate is the only one of its kind for a hydrolytic enzyme that contains a dinuclear active site.

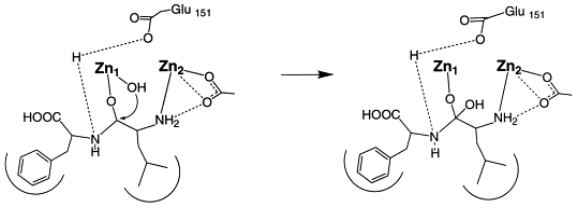

Scheme 5.

2.5. Placement of the nucleophilic hydroxide

Since AAP was shown to contain a bridging water/hydroxide by X-ray crystallography, the hypothesis that this water/hydroxide molecule is in fact the nucleophile in the hydrolytic reaction was tested by probing the inhibition of fluoride ions on AAPs catalytic process [40]. Monovalent anions such as fluoride have been used extensively to probe water or hydroxide binding to active site metal centers in metalloproteases [48], [78], [79], [80], [81], [82], [83], [84]. If the hydrolysis reaction is initiated by the bridging water/hydroxide, fluoride ions will displace the water/hydroxide at the active site and inhibit the reaction. Fluoride was found to be a pure uncompetitive inhibitor of AAP at pH 8.0 with a K_i of 30 mM. Thus, fluoride inactivates AAP only after substrate binding and only a single fluoride ion binds to AAP. These data indicate that substrate must bind prior to fluoride inhibition suggesting that the bridging water/hydroxide molecule becomes terminal after the coordination of substrate (Scheme 6). Between pH values of 6.0–9.0, fluoride acts as a pure uncompetitive inhibitor of AAP and the K_i increases from 1.2 to 370 mM. From a plot of pK_i versus pH, a pK_a value of 7.0±0.3 was extracted which corresponds to a single deprotonation process. The pK_a value of 7.0 reflects the Lewis acidity of the dizinc cluster in AAP.

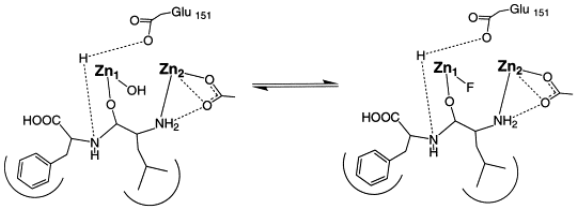

Scheme 6.

An interesting finding in this study was that chloride ions do not inhibit the action of AAP up to concentrations of 2 M at pH 8.0 [40]. The difference in fluoride and chloride inhibition behavior can be rationalized by inspection of the X-ray crystal structure of AAP and the relative hardness of the two halide bases. In AAP, the two Zn(II) ions reside in a carboxylate rich coordination environment and exhibit tetrahedral geometries [19]. This ligation sphere results in Zn(II) ions that are relatively hard acids [85]. It is well established that the relative order of binding of halide ions to hard acids is $F^- \gg Cl^- > Br^- > I^-$ [47], [85]. Therefore fluoride, as expected, binds to the Zn(II) ions in AAP more strongly than chloride ions. These data are in contrast to the mononuclear Zn(II) active sites in carboxypeptidase A and thermolysin, for example, that reside in histidine rich coordination environments and are inhibited by both fluoride and chloride ions [86], [87].

The dinuclear center in the native enzyme is structurally symmetric and AAP is ~80% active with only a single metal ion bound. These observations pose an important mechanistic question: what is the driving force to break the Zn2–OH(H) bond, leaving the putative nucleophile (OH^-) and the substrate on the same zinc (Zn1) ion? Several active site amino acid residues that do not act as Zn(II) ligands form hydrogen bonds within the active site. One of these, Glu151, contains an oxygen atom that in the AAP–BuBA complex is 3.0 Å from the coordinated N^{ε} nitrogen atom of His97, which is a ligand to Zn2 [75]. This distance is significantly shorter than the 3.4 Å distance found in the native structure and allows for a hydrogen bond between Glu151 and His97 that may not have existed in the native structure, or only existed weakly or transiently. These data suggest that Glu151 may regulate the Lewis acidity of Zn2. A second hydrogen-bonding interaction is observed between Asp99 and His97 forming an Asp–His–Zn triad. An oxygen atom of Asp99 is 2.7 Å from the N^{δ} nitrogen of His97 indicating a very strong hydrogen-bonding interaction. Strong hydrogen bonds between active site Asp residues and histidine ligands in zinc metalloproteins have been previously shown to provide a histidinate-like ligand, thus decreasing the Lewis acidity of Zn(II) ions [88]. For Zn2, coordination of Asp179 and Asp117 results in significant negative charge around the metal ion. Therefore, the hydrogen bond between His97 and Asp99 provides a histidinate like ligand that allows Zn2 to retain charge neutrality. If this hydrogen bond is sufficiently strong, which appears to be the case in the AAP–BuBA structure, this interaction may also decrease the Lewis acidity of Zn2 sufficiently to assist in the loss of the bridging water/hydroxide. The combination of these hydrogen-bonding interactions may, therefore, act to destroy the local symmetry of the dinuclear cluster as well as decrease the Lewis acidity of the Zn2 ion, allowing both the substrate and nucleophile to reside on the Zn1 site. Clarification of the catalytic role of these hydrogen-bonding interactions will require the preparation of site-directed mutants of these two amino acids.

2.6. The transition-state of peptide hydrolysis

The transition-state analog inhibitor l-leucinephosphonic acid (LPA) was shown to be a pure competitive inhibitor of both [ZnZn(AAP)] and [CoCo(AAP)] at pH 8.0 with K_i values of 6.6 and 5.5 μM, respectively [71]. The addition of LPA to [CoZn(AAP)], monitored by electronic absorption spectroscopy, resulted in an increase in the molar absorptivity from 58 to 68 M^{-1} cm^{-1} with no shift in the λ_{max} value of 525 nm [71], [89]. On the other hand, the addition of LPA to [ZnCo(AAP)] resulted in a clear shift in λ_{max} from 525 to 500 nm with a concomitant increase in the molar absorptivity to 63 M^{-1} cm^{-1}. However, the absorption spectrum of [ZnCo(AAP)]–LPA exhibited fine structure comprised of five absorption bands at 488, 517, 549, 579, and 601 nm. Electronic absorption fine structure is sometimes observed in severely distorted octahedral Co(II) species. Therefore, extensive distortions away from octahedral symmetry are likely responsible for the effects of LPA binding on the electronic absorption spectrum of [ZnCo(AAP)]. These data suggest that the first metal ion is five-coordinate, while the second metal ion resides in a very distorted six-coordinate environment. Taken together, these data reveal that LPA interacts with each metal ion in the dinuclear active site of AAP.

EPR studies of [CoZn(AAP)] and [ZnCo(AAP)], upon the addition of LPA, revealed that the two EPR signals observed in the resting enzymes, which arise from a pH-dependent mixture of species, are replaced by signals due to a single species [71], [89]. Simulation of these signals indicated that the Co(II) environments in both [CoZn(AAP)] and [ZnCo(AAP)] become highly asymmetrical and constrained upon the addition of LPA and clearly indicate interaction of LPA with both metal ions. Interestingly, the ^{59}Co hyperfine splitting for [ZnCo(AAP)]–LPA is significantly smaller than that observed for other Co(II)-substituted AAP species and suggests delocalization of some 30% of the paramagnetic electron density from the cobalt nucleus. These data imply a direct interaction of the Co(II) ion with an electrophilic moiety such as the N-terminal amine group of LPA which is also consistent with the anisotropy of g_{real} for this species. Moreover, upon the addition of LPA to [CoCo(AAP)], the perpendicular mode EPR signal disappears and an intense parallel-mode signal is observed with a crossover point at g_{eff}=10.3 at 9 K. These data indicate that the two S=3/2 Co(II) ions are ferromagnetically coupled upon

LPA binding. The signal exhibited maximum intensity at 4 K indicating that it is, in fact, a ground state transition. Based on the reported magnetic properties of several μ-aquo and μ-hydroxo dicobalt(II) model complexes, weak to moderately strong antiferromagnetic coupling is expected if LPA provides a single oxygen atom bridge [90], [91], [92], [93]. In addition, bis(μ-carboxylato) and tetrakis(μ-carboxylato)dicobalt(II) cores show weak antiferromagnetic spin-coupling. These data suggest that a single oxygen atom bridge is not present in the [CoCo(AAP)]–LPA complex and that the ferromagnetic spin–coupling interaction is not mediated through the carboxylate bridge. Since LPA interacts with both metal centers and a single oxygen atom bridge is likely absent, LPA appears to bind to the dicobalt(II) cluster of AAP as an η-1,2-μ-phosphonate with one ligand to the second Co(II) ion provided by the N-terminal amine.

The X-ray crystal structure of AAP bound by LPA was recently solved to 2.1 Å resolution (Fig. 8) [89]. Inhibitor binding does not introduce major conformational changes in the protein and the structures of native AAP and the AAP–LPA complex agree very well with an r.m.s. deviation of 0.21 Å for the 291 structurally equivalent C α-atoms. The two Zn(II) atoms are 3.9 Å apart in the LPA complex compared to 3.5 Å in the native structure (Fig. 9). The leucine group of LPA resides in a well-defined hydrophobic pocket adjacent to the dinuclear Zn(II) active site. The amino acid residues ligated to the dizinc(II) cluster are identical to those in the native structure with only minor perturbations in the bond lengths. Zn1 of the [ZnZn(AAP)]–LPA complex resides in a distorted tetrahedral environment while Zn2 exhibits a distorted five-coordinate geometry. Glu152 is coordinated in an asymmetric bidentate fashion to Zn1 with the additional oxygen atom providing a potential fifth ligand at a distance of 2.4 Å. Similarly, Asp179 is coordinated to Zn2 in an asymmetric bidentate fashion with the second oxygen atom residing 2.4 Å from the metal center providing a potential sixth ligand. Two of the LPA oxygen atoms are coordinated to the two Zn(II) ions in the active site. Namely, O1 is 1.9 Å from Zn1 and 3.4 Å from Zn2 while O3 is 3.3 Å from Zn1 and 2.3 Å from Zn2. There are no binding interactions between any single atom of LPA and both zinc ions; the phosphonate oxygen atom, O3, is coordinated to Zn2 and O1 is coordinated to Zn1. Interestingly, there is no electron density between the two Zn(II) ions suggesting that a bridging water molecule does not exist [89]. A hydrogen-bond (3.0 Å) also exists between Glu151 and the O3 oxygen atom of the phosphonate moiety. Since Glu151 also forms a hydrogen bond with the bridging water/hydroxide in the native structure, the O3 atom of the phosphonate group is likely in an analogous position to the nucleophilic oxygen atom. Finally, the NH_2 group of LPA, which mimics the N-terminal amine group of an incoming peptide, is 2.1 Å from Zn2. The X-ray crystallographic data indicates that LPA interacts with both metal centers and a single oxygen atom bridge is absent. Thus, LPA binds to the dinuclear active site of AAP as an η-1,2-μ-phosphonate with one ligand to the second metal ion provided by the N-terminal amine.

Fig. 8. Schematic of LPA bound to the dinuclear center AAP based on the coordinates from the Protein Data Bank (1FT7). The zinc ions are depicted as green spheres and LPA as red and yellow spheres.

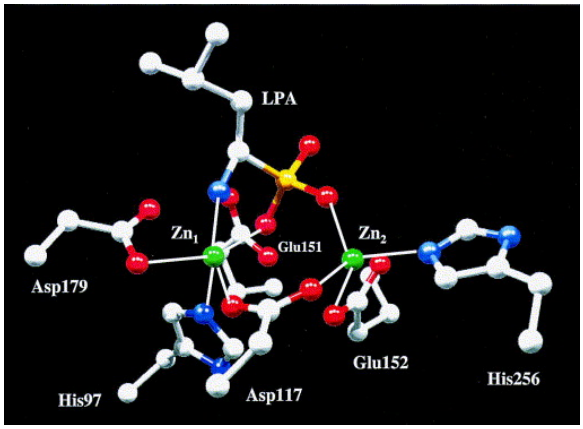

Fig. 9. Schematic of LPA bound to the dinuclear center AAP based on the coordinates 1FT7. LPA binds to the binuclear center with one of the ligands at Zn2 provided by the N-terminal amine and another by O3 of LPA. The LPA O1 atom provides a ligand to Zn1. The bridging water/hydroxyl molecule found in the native structure is not present in the AAP–LPA complex.

The S-atom of Met180, a residue in the hydrophobic pocket adjacent to the dinuclear active site of AAP, is only 3.1 Å from the N-terminal amine group of LPA, suggesting a hydrogen-bonding interaction [89]. Likewise, the O2 oxygen atom of Asp179 is 3.1 Å from the N-atom of the N-terminal amine group also indicating a hydrogen-bonding interaction. A similar interaction for the N-terminal amine of LPA has been shown by X-ray crystallography for LPA bound to blLAP [18]. The position of the N-terminal amine group in LPA is distinctly different than that observed for [ZnZn(AAP)] bound by d-iodophenylalaninehydroxamate (d-IPH) [63]. In the d-IPH complex, the N-terminal amine group is not present in the active site pocket but instead forms a hydrogen bond with Tyr-225 near the surface of the enzyme at the mouth of the active site pocket. Conversely, the N-terminal amine in the LPA complex is coordinated to Zn2. Therefore, the conformation of the inhibitor observed in the AAP-d-IPH complex is an inaccurate representation of the actual transition-state of peptide hydrolysis, i.e. the stereochemistry of the d-IPH inhibitor is incorrect for an actual peptide since IPH resides in the d-configuration. With this in mind, little mechanistic information can be gleaned from the [ZnZn(AAP)]–d-IPH

structure since d-IPH is simply acting as a metal chelator, rather than mimicking either substrate binding or the transition-state of the catalytic reaction. Consequently, any mechanistic conclusions derived from the AAP-d-IPH structure likely led to an incorrect assignment for the role of the second metal ion in the peptide hydrolysis reaction catalyzed by AAP [40], [51].

LPA provides an excellent mimic for the transition-state in the putative reaction pathway of peptide hydrolysis particularly because it resides in the correct l-configuration for peptide hydrolysis. Therefore, upon nucleophilic attack of the carbonyl sp^2 carbon atom of a peptide by an active site hydroxyl, the resultant sp^3 carbon-containing transition-state would be similar in structure to the R□PO_3 group of LPA (Scheme 7). The fact that no bridging water molecule is present in the AAP–LPA structure and that Glu151 forms a hydrogen bond with O3 of LPA (3.0 Å) is consistent with O3 being in the analogous position as the hydroxyl oxygen atom of the nucleophile. Glu151 has been previously implicated in the catalytic process from X-ray crystallographic data since Glu151 forms a hydrogen bond with the bridging water/hydroxide molecule in the resting enzyme [19]. The role of Glu151 is likely to assist in the deprotonation of the terminal water molecule to the nucleophilic hydroxo moiety, a role similar to that proposed for Glu270 in carboxypeptidase A [87]. The coordination of O3 to Zn2 suggests that after nucleophilic attack by the hydroxide ion, the resulting transition-state is stabilized by the additional binding interactions via the second metal ion in the dinuclear active site of AAP. These data suggest that the second metal ion in the dinuclear active site acts to stabilize the transition-state of hydrolysis, since a significantly greater number of binding interactions occur in the transition-state versus the substrate binding step.

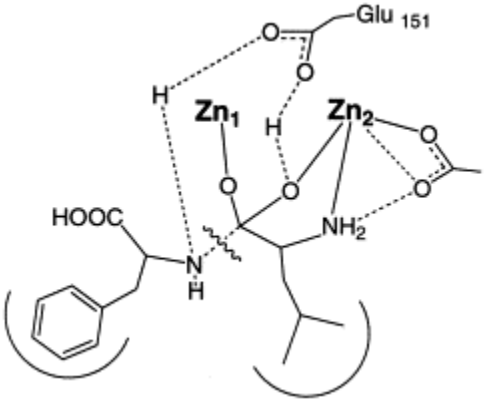

Scheme 7.

2.7. What is the rate-limiting step?

Since AAP is stable at 70 °C for a minimum of 5 h, the thermodynamic properties of AAP catalyzed hydrolysis of N-terminal amino acids was investigated [36]. AAP was found to be stable at 85 °C for ca. 1 min before loss in enzymatic activity was detected [40]. From these data, K_m values were derived at each temperature studied between 25 and 85 °C and was found to increase exponentially with increasing temperature. Moreover, the calculated V_{max} values were found to increase over this temperature range mimicking the K_m values. These data are very unusual since most enzymes undergo some denaturation at temperatures above 50 °C, resulting in a decrease in V_{max}. In a simple rapid equilibrium $V_{max}/[E]=k_p$, the first order rate constant [94]. Since the enzyme concentration was not altered over the course of the experiment, an Arrhenius plot was constructed by plotting ln k_{cat} versus $1/T$. A linear plot was obtained indicating that the rate-limiting step does not change over the temperature range 25–85 °C. These data also suggest that the rate-limiting step in AAP peptide hydrolysis is product formation. From the slope of the line, the activation energy (E_a) was calculated to be 36.5 kJ mol^{-1}. The enthalpy and entropy of activation at 25 °C calculated over the temperature range 298–358 K was found to be

34.0 kJ mol^{-1} and −94.2 J mol^{-1} K, respectively. The free energy of activation at 25 °C was found to be 62.1 kJ mol^{-1}.

The activation energy for the activated $ES^{‡}$ complex (36.5 KJ mol^{-1}) is similar to activation energies determined for pronase and both thermolysin and carboxypeptidase A [95], [96], [97]. The large positive enthalpy is indicative of a conformation change upon substrate binding, likely due to the energy of bond formation and breaking during nucleophilic attack on the scissile carbonyl carbon of the substrate. On the other hand, the large negative entropy value suggests that some of the molecular motions are lost upon $ES^{‡}$ complex formation, possibly due to hydrogen bond formation between Glu151 and/or Tyr225 (two amino acids recently implicated as catalytically important) and the substrate. All of these factors would contribute to the large positive free energy of activation.

Recently, k_{cat} values for l-*p*NA were measured at several different ratios of D_2O and H_2O at pH 8.0 [98]. The presence of D_2O substantially lowered the catalytic activity of AAP resulting in a solvent isotope effect of 2.75. For the simplest case, in which a single proton produces the solvent isotope effect, a plot of atom fraction of deuterium versus V_n/V_D should be linear [99], which was the case for l-*p*NA hydrolysis by AAP. These data suggest that a single proton transfer step occurs during the C□N bond-breaking step of peptide hydrolysis [100]. The solvent isotope effect observed for peptide cleavage by AAP is similar to the solvent isotope effect observed for carboxypeptidase A ($k_{cat}{}^{H}{}_2O/k_{cat}{}^{D}{}_2O$=1.9) [101] and the β-lactamase from *Bacteriodes fragilis* ($k_{cat}{}^{H}{}_2O/k_{cat}{}^{D}{}_2O$=2.59) [102]. The rate-limiting step in AAP peptide hydrolysis was previously suggested to be product formation [40]; therefore, the significant solvent isotope effect observed for peptide substrates likely represents the protonation of the leaving group, which facilitates the collapse of the transition-state. These data suggest that an active site residue, probably Glu151 based on X-ray crystallographic data, donates this proton back to the newly formed N-terminal amine to facilitate product formation (Scheme 8).

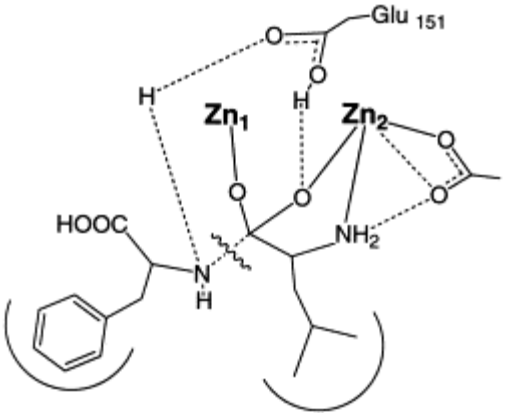

Scheme 8.

2.8. Mechanism of peptide hydrolysis by a dinuclear center

Combination of all of the kinetic, thermodynamic, spectroscopic, and X-ray crystallographic data has allowed a detailed mechanism of action to be proposed for the peptide hydrolysis reaction catalyzed by AAP (Fig. 10). Based on kinetic measurements of aliphatic alcohol binding to AAP, the incoming N-terminal peptide leucine group interacts with Phe244, Phe248, Tyr251, and Tyr225 in the hydrophobic pocket adjacent to the dinuclear active site [65]. This binding scheme is consistent with the large negative entropy and large positive enthalpy of activation reported for AAP [40]. An active site carboxylate group, Glu151, was implicated in the catalytic process from X-ray crystallographic data since Glu151 forms a hydrogen bond with the bridging water/hydroxide molecule in the resting enzyme [19]. It was proposed that the carbonyl oxygen atom of the incoming peptide binds to Zn1. These data are consistent with both EPR spectroscopic studies and the X-ray crystal structure of

AAP in the presence of the substrate-analog inhibitor BuBA which binds only to the first metal binding site [51], [54], [75]. Since AAP is ca. 80% active with only a single Zn(II) ion bound and fluoride binding occurs after substrate binding [40], it follows that the bridging water/hydroxide becomes terminal upon substrate binding and is bound to the first Zn(II) binding site. The breaking of the Zn2–OH(H) bond is likely assisted by N-terminal amine binding as well as Asp99 hydrogen-bonding to the Zn2 ligand, His97. Bertini et al. [46] have shown that an increase in coordination number from four to six for Zn(II) complexes with a bound water molecule steadily increases the energy of conversion between an hydroxo and water moiety. This increase in energy was related to an increase in pK_a, thus the higher the Zn(II) coordination number, the higher the pK_a. A similar trend is observed as the number of carboxylate ligands increases [46]. Therefore, the role of Glu151 is to assist in deprotonation of the terminal water molecule to the nucleophilic hydroxo moiety, similar to that of Glu270 in carboxypeptidase A [87]. At this point, the metal bound hydroxide can attack the activated carbonyl carbon of the peptide substrate forming a gem-diolate transition-state intermediate complex that is stabilized by coordination of both oxygen atoms to the dizinc(II) center, consistent with the [ZnZn(AAP)]–LPA structure. Glu151 can then provide an additional proton to the penultimate amino nitrogen returning it to its ionized state, consistent with recent kinetic isotope effect studies. The product-forming C–N bond-breaking step is likely the rate-limiting step, consistent with recent thermodynamic results [40]. Finally, the dizinc(II) cluster releases the cleaved peptides and adds a water molecule that bridges between the two metal ions. Thus, both metal ions are required for full enzymatic activity of AAP, but their individual roles appear to differ markedly.

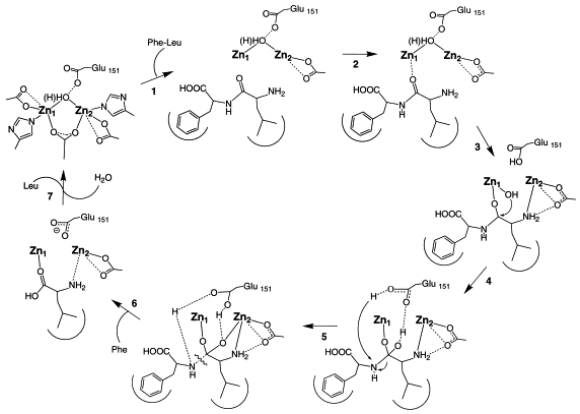

Fig. 10. Proposed mechanism of peptide hydrolysis catalyzed by AAP. Protein ligands to the metal ions are shown only in the first panel in order to avoid confusion.

2.9. Proposed mechanism when only one divalent metal ion is present

Since AAP retains ~80% of its activity with only a single Zn(II) ion present, it would appear that the proposal that the second metal ion stabilizes the transition-state is contradictory with the X-ray crystallographic results when there is a clear motif for a dinuclear metal-containing active site in AAP. Bennett and Holz [51] recently demonstrated that metal binding to apo-AAP occurs in a sequential fashion. It was also shown, based on electronic absorption and EPR spectroscopy, that the spectroscopic signatures for [Co_(AAP)] and [CoZn(AAP)] were identical but distinct from those of [ZnCo(AAP)]. The combination of these data with the X-ray crystallographic results of BuBA binding to AAP [75] indicate that the first metal binding site in AAP is the Zn1 site. Since AAP can function with only one metal ion present, the catalytic role of the second metal ion, must be replaced by another active site group or groups in its absence. Other hydrolases that contain dinuclear metallo-active sites, including aminopeptidases, have been shown to be catalytically competent with only one metal ion coordinated in a putative dinuclear site. For example, the MetAP from *E. coli* is fully active with only a single Co(II) or Fe(II) ion present even though the available X-ray crystallographic data suggests a dinuclear active site [103]. The divalent metal binding nature of MetAP and AAP also appear to be analogous to those of the zinc-

dependent β-lactamase from *B. cereus*. Of the two Zn(II) ions in the active site of the β-lactamase from *B. cereus*, the tightly bound Zn(II) ion is proposed to provide the nucleophile and also act as a Lewis acid to stabilize the tetrahedral transition-state [31], [104]. The role of the second Zn(II) ion is unclear since a conserved carboxylate residue is proposed to act as a general base to form the dianion and also to protonate the leaving group, thus, facilitating C□N bond cleavage. It has, therefore, been suggested that the *B. cereus* enzyme may be an evolutionary intermediate between mono- and dizinc(II) metallo-β-lactamases [105]. Similarly, X-ray crystallographic data for the MetAP from *E. coli* with a substrate-analogue inhibitor bound [106] revealed that the N-terminal amine nitrogen is coordinated to the non-catalytic Co(II) ion, that resides in the carboxylate-only side of the active site. For a single metal ion mechanism to occur, it was recently proposed [10] that the catalytic role ascribed to the second metal ion must be performed instead, by an active site amino acid group(s) (Scheme 9). For AAP, the carboxylate residue Asp179 forms a negatively charged pocket in the appropriate position to bind the N-terminal amine moiety. That the N-terminal amine can form a hydrogen bond with Asp179 comes from the X-ray crystal structures of AAP bound by BuBA and LPA [75], [89]. Thus, in the absence of a second divalent metal ion, the negatively charged pocket formed by Asp179 likely interacts with the N-terminal amine moiety to position the substrate similar to a Zn(II) ion if present.

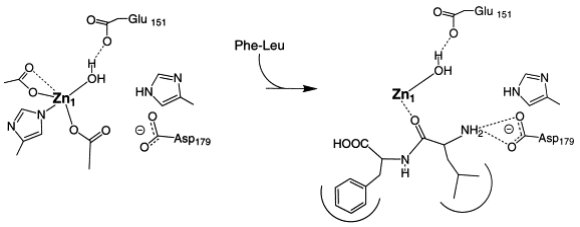

Scheme 9.

2.10. Inhibitor design

Because of the important physiological roles that aminopeptidases play, several laboratories have been interested in designing highly potent inhibitors for this class of enzyme that can function as both mechanistic probes and potential therapeutic agents. For AAP, several classes of relatively potent inhibitors have previously been investigated including the natural products amastatin (K_i=0.26 nM) and bestatin (K_i=18 nM), leucine halomethyl ketones (K_i=200–700 nM), BuBA (K_i=9600 nM), d-leucine hydroxamic acid (K_i=2.0 nM), and LPA (K_i=6600 nM) [18], [36], [43], [61], [68], [69], [70], [71], [72], [73], [74], [107], [108], [109]. A common feature of these inhibitors is that they all contain hydrophobic side chains and potential ligands that can coordinate to the metal ions in AAP. However, despite the wide-spread use of thiols in designing metalloenzyme inhibitors [110], [111], [112], the use of thiols as aminopeptidase inhibitors is rare [113], [114], [115]. Since thiols are known to be good ligands for Zn(II) cations [47], *N*-mercaptoacyl-leucyl-*p*-nitroanilide was recently synthesized, in anticipation that the N-terminal thiol would ligate to one or both of the Zn(II) ions in the AAP active site. Indeed, peptide thiols prove to be excellent inhibitors of AAP with the overall potencies (K_i*) of the inhibitors (Fig. 11) against AAP activity ranging from 2.5 to 57 nM [67]. These inhibition constants exceed that of the natural product bestatin and approach that of amastatin. The corresponding alcohols are simple competitive inhibitors of much lower potencies (K_i=23 and 360 μM). These data suggest that the free thiols are involved in the formation of the E▪I and E▪I* complexes, presumably serving as a metal ligand. As these peptide thiolate compounds are readily accessible by synthesis, they provide a novel class of potent aminopeptidase inhibitors.

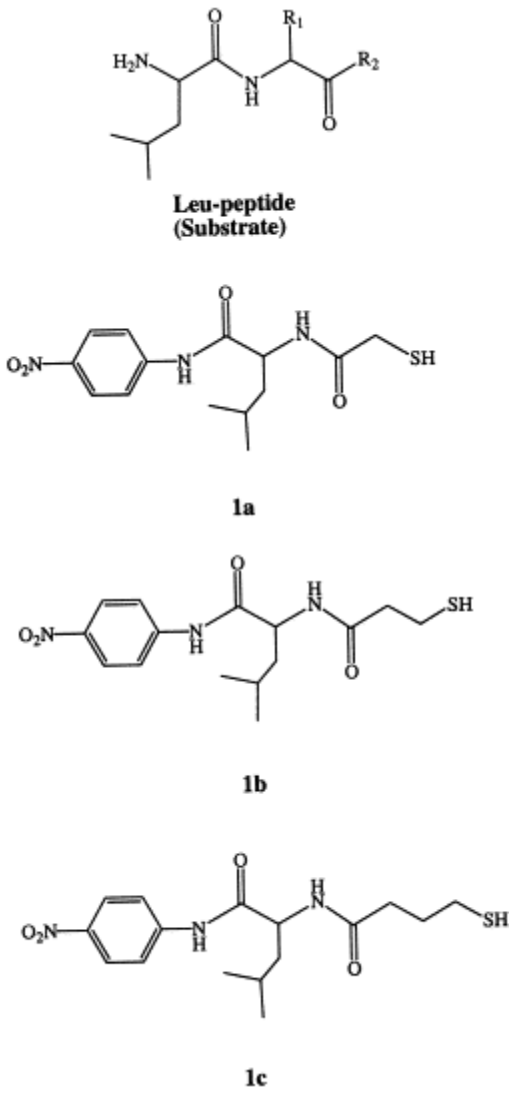

Fig. 11. Structures of AAP thiolate inhibitors.

The nature of the interaction of these thiol-based inhibitors with the dinuclear active site of AAP was investigated by electronic absorption and EPR spectroscopy of the various Co(II)-substituted derivatives of AAP. Combination of these data indicates that **1c** perturbs the electronic structure of both metal ions in the dinuclear active site of AAP. The EPR spectra of [CoCo(AAP)] also indicate that the Co□OH(H)□Co bridge is broken upon reaction with **1c**. Because the electronic structure of both metal ions is altered, and the Co□OH(H)□Co bridge is broken, it is tempting to propose that the thiol functionality of **1c** serves to replace the μ-OH(H) bridge and binds to form a Co□S(R)□Co moiety. However, the EPR data are not consistent with such a scenario. While one of the metal ions clearly undergoes a large electronic reorganization, consistent with sulfur ligation, the remaining metal ions display electronic symmetries not unlike those of the analogous, magnetically isolated Co(II) ions in the respective uncomplexed enzyme species. In systems of low symmetry, such as [CoCo(AAP)], [CoZn(AAP)], and [ZnCo(AAP)], significant changes in the electronic properties of the *S*=3/2 high-spin Co(II) ions are predicted. The observation that one of the Co(II) ions in all of the **1c**-complexed species of AAP studied retained an EPR signal indicative of low electronic symmetry which was only slightly perturbed from the analogous species in the respective resting enzyme, strongly argues against sulfur ligation to both divalent metal ions via a μ-S(R) bridge. In addition, the spin–spin interaction seen in resting [CoCo(AAP)] is abolished upon the addition of **1c** and, thus, it is unlikely that a single atom bridge is retained or established. Moreover, the lack of any decrease in the ^{59}Co

hyperfine splitting in the signals observed at high temperature (19 K) upon addition of **1c** indicates that there is no significant electron delocalization from one of the two active site metal ions.

Perhaps the most intriguing aspect of the complexation of **1c** by AAP is the fact that **1c** is a slow-binding inhibitor. The two metal ions in AAP have been shown to be electronically distinct [51], [54], [71], [75], [116] and, in the slow inhibitor binding step, one might expect that a preference for one or the other metal ion would be exhibited. Both the EPR and optical data, however, clearly indicate that either, but not both, of the metal ions can bind **1c** via the thiol functionality simultaneously (Fig. 12). These data imply a lack of exchangeability of the sulfur ligand once bound to the metal, entirely consistent with the very low inhibition constant of **1c**. The slow-binding process observed for thiol-containing inhibitors may, therefore, involve the non-selective coordination of the thiol moiety to one of the metal ions, followed by the slow deprotonation of the thiol group. Glu151 has been implicated as a general base in the catalytic reaction since it forms a hydrogen bond to the bridging water/hydroxide group in the resting enzyme; this residue may be responsible for the formation of the thiolate ion [19]. The reverse process, dissociation of the E_*I^* complex, would require protonation of the thiolate group.

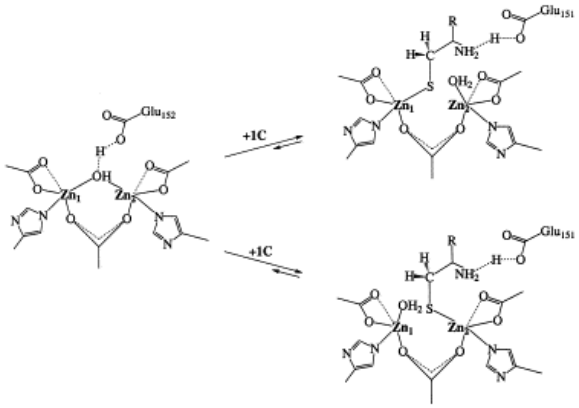

Fig. 12. Proposed binding scheme of **1c** with the dinuclear active site of AAP.

3. Concluding remarks

While AAP is not a specific target for pharmaceuticals at this time, a detailed understanding of its mechanism is still quite important with regard to other metallohydrolases that contain dinuclear active sites that are drug targets. Many of these enzymes are multimeric and/or cannot be obtained in large quantities for mechanistic studies. For example, the carboxypeptidase G_2 from *Pseudomonas* sp. strain RS-16 (CPG_2) is a dimeric enzyme of 42 kDa/subunit [23], [117]. CPG_2 catalyses the hydrolytic cleavage of reduced and non-reduced folates to pteroates and l-glutamate. The recent X-ray crystal structure of CPG_2 revealed a striking similarity between the catalytic domain of CPG_2 and AAP [19], [23]. CPG_2 contains two metal ions bound in its active site with a (μ-aquo)(μ-carboxylato)dizinc(II) core with one terminal carboxylate and one histidine residue at each metal site (Fig. 13) [23]. CPG_2s dinuclear active site is identical to that of AAPs even down to the coordination geometry of both metal ions, which is distorted tetrahedral. One of the potential medical uses of CPG_2 involves specific inhibitors for antibody-directed enzyme pro-drug therapy (ADEPT). In this procedure, a conjugate of the enzyme and an antibody specific to proteins present in tumor cells is administered, followed by the administration of a pro-drug with decreased toxicity compared to the actual drug. The pro-drug is converted to an active form of the drug and, thus, its action is limited to small area of cells with the conjugate attached to them [23].

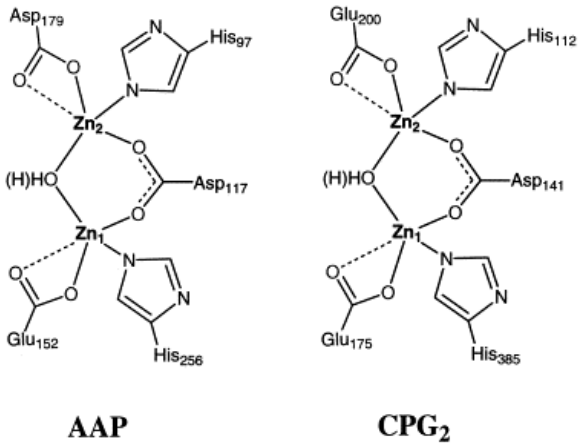

Fig. 13. Drawings of the active sites of [ZnZn(AAP)] and [ZnZn(CPG_2)] based on X-ray crystallography.

Another important pharmaceutical target, glutamate carboxypeptidase II (GCP II) is involved in the cleavage of glutamate from n-acetyl-l-aspartyl-l-glutamate (NAAG) [118]. GCP II has been found in the central and peripheral nervous system with gene expression primarily in astrocytes and is believed to play a role in modulating the release of glutamate. During conditions of acute injury (such as stroke) or chronic disease (such as diabetes), elevated glutamate levels in the synapses can incite a cascade of biochemical events that ultimately lead to cell injury and death. The cellular role of NAAG has been extensively studied and among other functions, it serves as a negative modulator of glutamatergic neurotransmission [119]. GCP II has been shown to require the presence of two zinc atoms for full catalytic activity. The X-ray crystal structure of a GCP II enzyme has not been reported, but based on sequence alignments with CPG_2 and AAP the catalytic domain of both of these enzymes is fully conserved in GCP II. For human GCP II, the ligands bound to the zinc ions are proposed to be His-377, Glu-425, Asp-453, His-553 and Asp-387 as the bridging moiety [120]. Glu-424 is postulated to be the general base in the active site, its mutation to Gln results in a decrease in V_{max} suggesting a role in catalysis. By analogy to AAP, the hydroxyl group of Tyr-552 in GCP II is potentially involved in the interaction with a phosphate group, as phosphate inhibition was perturbed in the Y552F mutant [120].

Finally, dapE-encoded *N*-succinyl-l,l-diaminopimelic acid desuccinylases (dapEs), have been shown to require two Zn(II) ions for full enzymatic activity [121]. DapEs catalyze the hydrolysis of *N*-succinyl-l,l-diaminopimelic acid, forming l,l-diaminopimelic acid and succinate and are members of the *meso*-diaminopimelate (mDAP)/lysine biosynthetic pathway [121]. DapEs have been purified from *E. coli* and *Haemophilus influenzae* while the genes that encode for dapEs have been sequenced from *Corynebacterium glutamicum*, *Helicobacter pylori* and *Mycobacterium tuberculosis*. The dapEs from *E. coli* and *H. influenzae* have been overexpressed in *E. coli* and purified to homogeneity [121], [122]. Alignment of all of the known gene sequences for dapE enzymes identified several residues that are highly conserved in metal-containing hydrolytic enzymes with co-catalytic active sites. Further alignment with the structurally characterized enzymes AAP and CPG_2 indicated that all of the amino acids that function as metal ligands are strictly conserved [19], [23], [121], [123]. Similar to AAP, the as purified dapE enzyme contains only one tightly bound Zn(II) ion and exhibits ~80% of the maximum enzymatic activity [36]. The importance of understanding the mechanism of action of dapE enzymes is underscored by the emergence of several pathogenic bacterial strains that are resistant to all currently available antibiotics [124], [125], [126], [127]. Since one of the products of mDAP/lysine biosynthetic pathway, lysine, is required in protein synthesis while both products, mDAP and lysine are essential components of the peptidoglycan cell wall for Gram-negative and some Gram-positive bacteria, inhibitors of dapEs may provide a new class of antibiotics. Inhibitors of peptidoglycan biosynthesis (β-lactams, including vancomycin) have proven to be very potent antibiotics; evidence that interfering with cell wall

synthesis can have deleterious effects on bacterial cell survival [126]. The fact that there are no similar pathways in mammals suggests that inhibitors of enzymes in the mDAP/lysine pathway may provide selective toxicity against bacteria and have little or no effect on humans.

Therefore, while AAP is a prototypical hydrolase that contains a dinuclear active site, it is an exciting and important enzyme from both an inorganic/catalytic perspective as well as from a medicinal viewpoint. The proposed mechanism of action for AAP provides a blueprint for the catalytic mechanisms of CPG_2, GCP II, and dapE as well as several other hydrolases with dinuclear active sites. All of these enzymes are attractive targets for inhibitors that may provide new treatments for bacterial infections, cancer, and neurological disorders. Moreover, the information obtained from the characterization of a detailed mechanism of action for AAP should aid in the rational design of such drugs.

Acknowledgements

This work was supported by the National Science Foundation (CHE-9816487 and CHE-9422098) and the National Institutes of Health (GM-56495).

References

[1] N. Sträter, W.N. Lipscomb, T. Klabunde, B. Krebs. *Angew. Chem. Int. Ed. Engl*., 35 (1996), p. 2024
[2] W.N. Lipscomb, N. Sträter. *Chem. Rev*., 96 (1996), p. 2375
[3] D.E. Wilcox. *Chem. Rev*., 96 (1996), p. 2435
[4] G.C. Dismukes. *Chem. Rev*., 96 (1996), p. 2909
[5] R.P. Hausinger. *Biochemistry of Nickel*, New York: Plenum Press (1993)
[6] J. Chin. *Acc. Chem. Res*., 24 (1991), p. 145
[7] K. Lai, K.I. Dave, J.R. Wild. *J. Biol. Chem*., 269 (1994), p. 16579
[8] F.M. Menger, L.H. Gan, E. Johnson, D.H. Durst. *J. Am. Chem. Soc*., 109 (1987), p. 2800
[9] J. Taunton. *Chem. Biol*., 4 (1997), p. 493
[10] E.C. Griffith, Z. Su, B.E. Turk, S. Chen, Y.-H. Chang, Z. Wu, K. Biemann, J.O. Liu. *Chem. Biol*., 4 (1997), p. 461
[11] N. Sin, L. Meng, M.Q. Wang, J.J. Wen, W.G. Bornmann, C.M. Crews. *Proc. Natl. Acad. Sci. USA*, 94 (1997), p. 6099
[12] W.T. Lowther, D.A. McMillen, A.M. Orville, B.W. Matthews. *Proc. Natl. Acad. Sci. USA*, 95 (1998), p. 12153
[13] S. Liu, J. Widom, C.W. Kemp, C.M. Crews, J. Clardy. *Science*, 282 (1998), p. 1324
[14] G. Pulido-Cejudo, B. Conway, P. Proulx, R. Brown, C.A. Izaguirre. *Antiviral Res*., 36 (1997), p. 167
[15] B.L. Vallee, D.S. Auld. *Biochemistry*, 29 (1990), p. 5647
[16] B.L. Vallee, D.S. Auld. *Proc. Natl. Acad. Sci. USA*, 90 (1993), p. 2715
[17] B.L. Vallee, D.S. Auld. *Biochemistry* (1993), p. 6493
[18] N. Sträter, W.N. Lipscomb. *Biochemisty*, 34 (1995), p. 9200
[19] B. Chevrier, C. Schalk, H. D'Orchymont, J.-M. Rondeau, D. Moras, C. Tarnus. *Structure*, 2 (1994), p. 283
[20] H.M. Greenblatt, O. Almog, B. Maras, A. Spungin-Bialik, D. Barra, S. Blumberg, G. Shoham. *J. Mol. Biol*., 265 (1997), p. 620
[21] M.C.J. Wilce, C.S. Bond, N.E. Dixon, H.C. Freeman, J.M. Guss, P.E. Lilley, J.A. Wilce. *Proc. Natl. Acad. Sci. USA*, 95 (1998), p. 3472
[22] T.W. Lowther, Y. Zhang, P.B. Sampson, J.F. Honek, B.W. Matthews, Biochemistry 38 (1999), in press.
[23] S. Rowsell, R.A. Pauptit, A.D. Tucker, R.G. Melton, D.M. Blow, P. Brick. *Structure*, 5 (1997), p. 337
[24] E.E. Kim, H.W. Wyckoff. *J. Mol. Biol*., 218 (1991), p. 449
[25] E. Hough, L.K. Hansen, B. Birknes, K. Jynge, S. Hansen, A. Horvik, C. Little, E. Dodson, Z. Derewenda. *Nature*, 338 (1989), p. 357
[26] A. Volbeda, A. Lahm, F. Sakiyama, D. Suck. *EMBO J*., 10 (1991), p. 1607

[27] N. Sträter, T. Klabunde, P. Tucker, H. Witzel, B. Krebs. *Science*, 268 (1995), p. 1489
[28] M.M. Benning, J.M. Kuo, F.M. Raushel, H.M. Holden. *Biochemistry*, 34 (1995), p. 7973
[29] Z.F. Kanyo, L.R. Scolnick, D.E. Ash, D.W. Christianson. *Nature*, 383 (1996), p. 554
[30] L. Lebioda, B. Stec. *J. Am. Chem. Soc*., 111 (1989), p. 8511
[31] N.O. Concha, B.A. Rasmussen, K. Bush, O. Hertzberg. *Structure*, 4 (1996), p. 823
[32] E. Jabri, M.B. Carr, R.P. Hausinger, P.A. Karplus. *Science*, 268 (1995), p. 998
[33] A. Taylor. *FASEB J*., 7 (1993), p. 290
[34] A. Taylor. *TIBS*, 18 (1993), p. 167
[35] A. Taylor. *Aminopeptidases*, R.G. Landes Co, Austin, TX, USA (1996)
[36] J.M. Prescott, S.H. Wilkes. *Methods Enzymol*., 45B (1976), p. 530
[37] N. Sträter, W.N. Lipscomb. *Biochemisty*, 34 (1995), p. 14792
[38] A. Taylor, K.W. Volz, W.N. Lipscomb, L.J. Takemoto. *J. Biol. Chem*., 259 (1984), p. 14757
[39] J.M. Prescott, S.H. Wilkes. *Arch. Biochem. Biophys*., 117 (1966), p. 328
[40] G. Chen, T. Edwards, V.M. D'souza, R.C. Holz. *Biochemistry*, 36 (1997), p. 4278
[41] J.M. Prescott, S.H. Wilkes, F.W. Wagner, K.J. Wilson. *J. Biol. Chem*., 246 (1971), p. 1756
[42] Z.-Z. Zhang, S. Nirasawa, Y. Nakajima, M. Yoshida, K. Hayashi. *Biochem. J*., 350 (2000), p. 671
[43] J.O. Baker, J.M. Prescott. *Biochemistry*, 22 (1983), p. 5322
[44] J.M. Prescott, F.W. Wagner, B. Holmquist, B.L. Vallee. *Biochem. Biophys. Res. Commun*., 114 (1983), p. 646
[45] M.E. Bayliss, J.M. Prescott. *Biochemistry*, 25 (1986), p. 8113
[46] I. Bertini, C. Luchinat, M. Rosi, A. Sgamellotti, F. Tarantelli. *Inorg. Chem*., 29 (1990), p. 1460
[47] F.A. Cotton, G. Wilkinson, C.A. Murillo, M. Bochmann. *Advanced Inorganic Chemistry*, Wiley, New York (1999)
[48] I. Bertini, C. Luchinat. *Adv. Inorg. Biochem*., 6 (1984), p. 71
[49] R.H. Holm, P. Kennepohl, E.I. Solomon. *Chem. Rev*., 96 (1996), p. 2239
[50] J.M. Prescott, F.W. Wagner, B. Holmquist, B.L. Vallee. *Biochemistry*, 24 (1985), p. 5350
[51] B. Bennett, R.C. Holz. *J. Am. Chem. Soc*., 119 (1997), p. 1923
[52] T.E. Elgren, L.-J. Ming, L. Que. *Inorg. Chem*., 33 (1994), p. 891
[53] W. Horrocks, I. DeW Jr., B. Holmqust, J.S. Thompson. *J. Inorg. Chem*., 12 (1980), p. 131
[54] B. Bennett, R.C. Holz. *Biochemistry*, 36 (1997), p. 9837
[55] R.S. Drago. *Physical Methods for Chemists*, Saunders, Orlano, FL (1992)
[56] M.T. Werth, S.-F. Tang, G. Formicka, M. Zeppezauer, M.K. Johnson. *Inorg. Chem*., 34 (1995), p. 218
[57] J.R. Pilbrow, G.R. Hanson, *Metallobiochemistry*, 1993, 330pp.
[58] F.W. Wagner, S.H. Wilkes, J.M. Prescott. *J. Biol. Chem*., 247 (1972), p. 1208
[59] A. Spungin, S. Blumberg. *Eur. J. Biochem*., 183 (1989), p. 471
[60] D. Ben-Meir, A. Spungin, R. Ashkenazi, S. Blumberg. *Eur. J. Biochem*., 212 (1993), p. 107
[61] H. Kim, W.N. Lipscomb. *Biochemistry*, 32 (1993), p. 8465
[62] M.P. Allen, A.H. Yamada, F.H. Carpenter. *Biochemistry*, 22 (1983), p. 3778
[63] B. Chevrier, H. D'Orchymont, C. Schalk, C. Tarnus, D. Moras. *Eur. J. Biochem*., 237 (1996), p. 393
[64] K. Mäkinen, P.-L. Mäkinen, S.H. Wilkes, M.E. Bayliss, J.M. Prescott. *Eur. J. Biochem*., 128 (1982), p. 257
[65] L. Ustynyuk, B. Bennett, T. Edwards, R.C. Holz. *Biochemistry*, 38 (1999), p. 11433
[66] D. Bienvenue, B. Bennett, R.C. Holz. *J. Inorg. Biochem*., 78 (2000), p. 43
[67] K.M. Huntington, D. Bienvenue, Y. Wei, B. Bennett, R.C. Holz, D. Pei. *Biochemistry*, 38 (1999), p. 15587
[68] J.O. Baker, S.H. Wilkes, M.E. Bayliss, J.M. Prescott. *Biochemistry*, 22 (1983), p. 2098
[69] J.O. Baker, J.M. Prescott. *Biochem. Biophys. Res. Commun*., 130 (1985), p. 1154
[70] B. Lejczak, P. Kafarski, J. Zygmunt. *Biochemistry*, 28 (1989), p. 3549
[71] B. Bennett, R.C. Holz. *J. Am. Chem. Soc*., 120 (1998), p. 12139
[72] S.H. Wilkes, J.M. Prescott. *J. Biol. Chem*., 258 (1983), p. 13517

[73] .S.H. Wilkes, J.M. Prescott. *J. Biol. Chem*., 262 (1987), p. 8621
[74] W.W.-C. Chan, P. Dennis, W. Demmer, K. Brand. *J. Biol. Chem*., 257 (1982), p. 7955
[75] C. DePaola, B. Bennett, R.C. Holz, D. Ringe, G. Petsko. *Biochemistry*, 38 (1999), p. 9048
[76] C.A. Kettner, A.B. Shenvi. *J. Biol. Chem*., 259 (1984), p. 15106
[77] L.H. Takahashi, R. Radhakrishnan, R.E.J. Rosenfield, E.F.J. Meyer. *Biochemistry*, 28 (1989), p. 7610
[78] B.L. Vallee, A. Galdes. *Adv. Enzymol*., 56 (1984), p. 283
[79] A.C. Williams, D.S. Auld. *Biochemistry*, 25 (1986), p. 94
[80] J.J. Yang, D.R. Artis, H.E. Van Wart. *Biochemistry*, 33 (1994), p. 6516
[81] M.E. Lee, T. Nowak. *Biochemistry*, 31 (1992), p. 2172
[82] J.B. Vincent, M.W. Crowder, B.A. Averill. *Biochemistry*, 30 (1991), p. 3025
[83] N.E. Dixon, R.L. Blakely, B. Zerner. *Can. J. Biochem*., 58 (1980), p. 481
[84] A.J. Ganzhorn, M.-C. Chanal. *Biochemistry*, 29 (1990), p. 6065
[85] A.E. Martell, R.D. Hancock, Plenum Press, New York, 1996, 199pp.
[86] B.W. Matthews. *Acc. Chem. Res*., 21 (1988), p. 333
[87] D.W. Christianson, W.N. Lipscomb. *Acc. Chem. Res*., 22 (1989), p. 62
[88] D.W. Christianson, R.S. Alexander. *J. Am. Chem. Soc*., 111 (1989), p. 6412
[89] C. Stamper, B. Bennett, T. Edwards, R.C. Holz, D. Ringe, G. Petsko. *Biochemistry*, 40 (2001), p. 7035
[90] V.T. Kalinnikov, Y.V. Rakitin, W.E. Hatfield. *Inorg. Chim. Acta*, 31 (1978), p. 1
[91] U. Turpeinen, M. Ahlgren, R. Hämäläinen. *Acta Crystallogr*., B32 (1982), p. 1580
[92] U. Turpeinen, R. Hämäläinen, J. Reedijk. *Polyhedron*, 6 (1987), p. 1603
[93] I.R. Little, B.P. Straughan, P. Thornton. *J. Chem. Soc. Dalton. Trans*. (1986), p. 2211
[94] I.H. Segel. *Enzyme Kinetics: Behavior and Analysis of Rapid Equilibrium and Steady-state Enzyme Systems*, Wiley, New York (1975)
[95] R. Lumry, E.L. Smith, R.R. Glantz. *J. Am. Chem. Soc*., 73 (1951), p. 4330
[96] S. Kunugi, H. Hirohara, N. Ise. *Eur. J. Biochem*., 124 (1982), p. 157
[97] C.-H. Wu, W.-Y. Lin. *J. Inorg. Biochem*., 57 (1995), p. 79
[98] D.L. Bienvenue, R.S. Mathew, D. Ringe, R.C. Holz, J. *Biol. Inorg. Chem*. 2001, in press.
[99] J.P. Elrod, J.L. Hogg, D.M. Quinn, K.S. Venkatasubban, R.L. Schowen. *J. Am. Chem. Soc*., 102 (1980), p. 3917
[100] W.W. Cleland. *Crit. Rev. Biochem*., 13 (1982), p. 385
[101] M.W. Makinen, L.C. Kuo, J.J. Dymowski, S. Jaffer. *J. Biol. Chem*., 254 (1979), p. 356
[102] Z. Wang, S.J. Benkovic. *J. Biol. Chem*., 273 (1998), p. 22402
[103] V.M. D'souza, B. Bennett, R.C. Holz. *Biochemistry*, 39 (2000), p. 3817
[104] S. Bounaga, A.P. Laws, M. Galleni, M.I. Page. *Biochem. J*., 331 (1998), p. 703
[105] S.M. Fabiane, M.K. Sohi, T. Wan, D.J. Payne, J.H. Bateson, T. Mitchell, B.J. Sutton. *Biochemistry*, 37 (1998), p. 12404
[106] W.T. Lowther, A.M. Orville, D.T. Madden, S. Lim, D.H. Rich, B.W. Matthews. *Biochemistry*, 38 (1999), p. 7678
[107] A. Taylor, C.Z. Peltier, F.J. Torre, N. Hakamian. *Biochemistry*, 32 (1993), p. 784
[108] S.H. Wilkes, J.M. Prescott. *J. Biol. Chem*., 260 (1985), p. 13154
[109] S.K. Burley, P.R. David, R.M. Sweet, A. Taylor, W.N. Lipscomb. *J. Mol. Biol*., 224 (1992), p. 113
[110] D.W. Cushman, H.S. Cheung, E.F. Sabo, M.A. Ondetti. *Biochemistry*, 16 (1977), p. 5484
[111] M.A. Ondetti, M.E. Condon, J. Reid, E.F. Sabo, H.S. Cheung, D.W. Cushman. *Biochemistry*, 18 (1979), p. 1427
[112] M.M. Murphy, J.R. Schullek, E.M. Gordon, M.A. Gallop. *J. Am. Chem. Soc*., 117 (1995), p. 7029
[113] W.W.-C. Chan. *Biochem. Biophys. Res. Commun*., 116 (1983), p. 297
[114] E.M. Gordon, J.D. Godfrey, N.G. Delaney, M.M. Asaad, D. Von Langen, D.W. Cushman. *J. Med. Chem*., 31 (1988), p. 2199

[115] R.E. Beattie, D.T. Elmore, C.H. Williams, D.J.S. Guthrie. *Biochem. J.*, 245 (1987), p. 285
[116] X.-M. Chen, T.-X. Tong, T.C.W. Mak. *Inorg. Chem*., 33 (1994), p. 4586
[117] R.F. Sherwood, R.G. Melton, S.M. Alwan, P. Hughes. *Eur. J. Biochem*., 148 (1985), p. 447
[118] M.B. Robinson, R.D. Blakely, R. Couto, J.t. Coyle. *J. Biol. Chem*., 262 (1987), p. 14498
[119] R. Luthi-Carter, A.K. Barczak, H. Speno, J.T. Coyle. *Brain Res*., 795 (1998), p. 341
[120] H.S. Speno, R. Luthi-Carter, W.L. Macias, S.L. Valentine, A.R.T. Joshi, J.T. Coyle. *Mol. Pharmacol*., 55 (1999), p. 179
[121]. T.L. Born, R. Zheng, J.S. Blanchard. *Biochemistry*, 37 (1998), p. 10478
[122] J. Bouvier, C. Richaud, W. Higgins, O. Bögler, P. Stragier. *J. Bacteriol*., 174 (1992), p. 5265
[123] S. Makarova, N.V. Grishin. *J. Mol. Biol*., 292 (1999), p. 11
[124] CDC Prevention, *Mor. Mortal. Wkly Rep*. 44 (1995) 1.
[125] R.A. Howe, K.E. Bowker, T.R. Walsh, T.G. Feest, A.P. MacGowan. *Lancet*, 351 (1997), p. 601
[126] S.B. Levy. *Sci. Am*., 278 (1998), p. 46
[127] J. Chin. *New Sci*., 152 (1996), p. 32